© 2017. Published by The Company of Biologists Ltd | Development (2017) 144, 2469-2479 doi:10.1242/dev.147025

RESEARCH ARTICLE

Altered feto-placental vascularization, feto-placental malperfusion and fetal growth restriction in mice with *Egfl7* loss of function

Lauretta A. Lacko[1,*], Romulo Hurtado[2], Samantha Hinds[1], Michael G. Poulos[3], Jason M. Butler[3] and Heidi Stuhlmann[1,*]

ABSTRACT

EGFL7 is a secreted angiogenic factor produced by embryonic endothelial cells. To understand its role in placental development, we established a novel *Egfl7* knockout mouse. The mutant mice have gross defects in chorioallantoic branching morphogenesis and placental vascular patterning. Microangiography and 3D imaging revealed patchy perfusion of *Egfl7*$^{-/-}$ placentas marked by impeded blood conductance through sites of narrowed vessels. Consistent with poor feto-placental perfusion, *Egfl7* knockout resulted in reduced placental weight and fetal growth restriction. The placentas also showed abnormal fetal vessel patterning and over 50% reduction in fetal blood space. *In vitro*, placental endothelial cells were deficient in migration, cord formation and sprouting. Expression of genes involved in branching morphogenesis, *Gcm1*, *Syna* and *Synb*, and in patterning of the extracellular matrix, *Mmrn1*, were temporally dysregulated in the placentas. *Egfl7* knockout did not affect expression of the microRNA embedded within intron 7. Collectively, these data reveal that *Egfl7* is crucial for placental vascularization and embryonic growth, and may provide insight into etiological factors underlying placental pathologies associated with intrauterine growth restriction, which is a significant cause of infant morbidity and mortality.

KEY WORDS: Egfl7, Placenta, Branching morphogenesis, Endothelial dysfunction, Mmrn1, Gcm1

INTRODUCTION

The placenta provides the interface between the fetal and maternal circulatory systems during pregnancy, performing essential gas and nutrient exchange, as well as immunological and endocrine functions that are crucial for mammalian embryonic development. Proper development of the placenta requires coordinated maternal vascular remodeling and fetal vasculogenesis to bring the two circulatory systems into close contact. Defects in these processes can result in placental pathologies, including pre-eclampsia (PE) and intrauterine growth restriction (IUGR), which are leading causes of maternal and fetal morbidity and mortality (Young et al., 2010; Sharma et al., 2016a). Moreover, IUGR has been linked to significant morbidities later in life, such as coronary heart disease, diabetes mellitus and hyperinsulinemia (Sharma et al., 2016b). Despite this, the molecular factors and signaling pathways controlling placental development remain incompletely understood.

The site of exchange between the mother and the fetus occurs in the chorionic villi in humans and in the analogous fetal labyrinth zone in mice. Labyrinth formation requires a series of morphogenetic events, including chorionic branching morphogenesis and subsequent blood vessel development (Rossant and Cross, 2001). The fetal vasculature of the placenta is derived from extra-embryonic mesodermal cells of the allantois. The allantois makes contact with chorionic trophoblast cells, which develop extensive folds into which blood vessels invade and interdigitate, forming a highly branched fetal vascular network of the mature placenta (Rossant and Cross, 2001; Watson and Cross, 2005).

Epidermal growth factor like domain 7 (*Egfl7*) encodes a secreted angiogenic factor whose expression is largely restricted to the endothelium in the developing embryo, and is downregulated in the adult quiescent endothelium. A long-standing controversy concerning the specific endothelial functions of *Egfl7* and its intronic microRNA, miR-126, is based on conflicting results from knockout and knockdown studies in mice and zebrafish (Kuhnert et al., 2008; Wang et al., 2008). Earlier work demonstrated that specific loss of miR-126 in mice and zebrafish results in angiogenesis defects that were originally attributed to loss of function of *Egfl7*. Furthermore, *egfl7* morphant zebrafish display severe vascular defects, whereas embryos of *egfl7* mutant zebrafish and one *Egfl7*-specific knockout mouse line do not show obvious phenotypes, owing to activation of compensatory genes (Fish et al., 2008; Kuhnert et al., 2008; Nichol and Stuhlmann, 2012; Rossi et al., 2015; Wang et al., 2008). Conversely, endothelial-specific overexpression of Egfl7 in mice results in vascular defects during embryogenesis and pathological vascularization in the neonatal retina (Nichol et al., 2010; Bambino et al., 2014), suggesting a specific role for *Egfl7* in vascular development.

Of importance for this study, *Egfl7* is expressed in the inner cell mass and trophectoderm of mouse blastocysts, in the allantois, as well as in endothelial cells (ECs) and spongiotrophoblast cells of the developing placenta (Lacko et al., 2014; Bambino et al., 2014; Campagnolo et al., 2008; Fitch et al., 2004; Parker et al., 2004; Soncin et al., 2003). Egfl7 has been shown to promote migration of ECs and trophoblast cells (Campagnolo et al., 2005; Massimiani et al., 2015; Nichol et al., 2010). Its expression is downregulated in human pre-eclamptic placentas (Lacko et al., 2014; Junus et al., 2012), placentas of a mouse model of PE prior to the onset of clinical signs (Lacko et al., 2014), and in plasma of individuals with pregnancies affected by intrauterine growth restriction (Zanello et al., 2013).

Here, we have developed a novel *Egfl7* loss-of-function mouse model (*Egfl7*$^{-/-}$) that maintains miR-126 expression to study the functional role of *Egfl7* during placental development. We

[1]Department of Cell and Developmental Biology, Weill Cornell Medical College, 1300 York Avenue, Box 60, New York, NY 10065, USA. [2]Department of Physiology and Biophysics, Weill Cornell Medical College, 1300 York Avenue, Box 60, New York, NY 10065, USA. [3]Department of Medicine, Weill Cornell Medical College, 1300 York Avenue, Box 60, New York, NY 10065, USA.

*Authors for correspondence (hes2011@med.cornell.edu; lal2018@med.cornell.edu)

H.S., 0000-0001-7217-768X

Received 17 November 2016; Accepted 16 May 2017

Development (2017) 144, 2469-2479 doi:10.1242/dev.147025

demonstrate gross vascular patterning defects, EC dysfunction and feto-placental malperfusion at sites of narrowed fetal capillaries in *Egfl7*$^{-/-}$ placentas, which result in fetal growth restriction of *Egfl7*$^{-/-}$ embryos. We establish, for the first time, that *Egfl7* loss of function results in dysregulation of genes that regulate chorioallantoic branching morphogenesis and labyrinth formation (*Gcm1*, *Syna* and *Synb*), and downregulation of the extracellular matrix gene *Mmrn1*. Our results demonstrate a crucial role for *Egfl7* in normal development of the placenta and show vascular-specific defects in *Egfl7*-specific knockout mice.

RESULTS

Generation of *Egfl7* loss-of-function mice

To analyze the function of *Egfl7* during development, we generated a global *Egfl7* loss-of-function mouse model that maintains expression of miR-126, the microRNA embedded in intron 7 (*Egfl7*$^{-/-}$). Blastocysts were injected with an *Egfl7* knockout embryonic stem cell clone (VelociGene modified allele ID1501) that was produced at Regeneron Pharmaceuticals using VelociGene methods (Valenzuela et al., 2003). A 13 bp region in exon 3 from the first ATG to 1 bp after the second ATG (5′-ATG CAG ACC ATG T-3′) in the targeted *Egfl7* allele was replaced with a hygromycin LacZless-Poly-A-less cassette flanked by two loxP sites (Fig. 1A,B). Founder mice were backcrossed for ten generations into a C57BL/6J congenic background. Males heterozygous for the modified *Egfl7* allele were mated with females carrying a CAG-Cre transgene (Sakai and Miyazaki, 1997), the Cre recombinase activity of which is maintained in mature oocytes regardless of Cre transgene transmission. Offspring with the excised hygromycin cassette that lacked the CAG-Cre transgene were intercrossed to obtain *Egfl7*$^{-/-}$ pups. Sequencing of genomic DNA from *Egfl7*$^{+/+}$ and *Egfl7*$^{-/-}$ mice confirmed the Cre-mediated excision and deletion of the MQTM-coding sequence. The deletion leaves a single in-frame ATG (position 598 in the coding sequence) located C-terminal to the crucial functional domains of EGFL7, including the signal peptide, the EMI domain and the two EGF domains.

To confirm the specific loss of Egfl7 and maintenance of miR126, we determined their expression levels. Egfl7 transcripts were measured in E12.5 placentas from C57BL/6J and *Egfl7*$^{-/-}$ mice by real time RT-PCR using two sets of primers: one set complimentary to sequences in exons 8 (forward) and exon 9 (reverse) (Fig. 1A, blue); and a second pair with the forward primer containing the 13 bp sequence in exon 3 targeted for deletion in the *Egfl7*$^{-/-}$ mice and the reverse primer complimentary to a sequence in exon 4 (Fig. 1A, green). As predicted, Egfl7 transcripts containing exons 8 and 9 sequences were detected at similar levels in both C57BL/6J and *Egfl7*$^{-/-}$ placentas. In contrast, the Egfl7 transcript that was amplified with the forward primer complimentary to the sequence encoding the two translational start sites was detected at high levels in C57BL/6J placentas, but was absent in *Egfl7*$^{-/-}$ placentas (Fig. 1C,D). Deletion of the translational start codon of *Egfl7* is predicted to have no effect on production of miR-126. Indeed, real time RT-PCR of E12.5 C57BL/6J and *Egfl7*$^{-/-}$ placentas demonstrates no significant difference in miR-126-3p and miR-126-5p expression levels (Fig. 1E,F).

Egfl7 loss of function results in reduced placental weights and fetal growth restriction

Initial analyses of mice with the targeted allele were performed using *Egfl7*$^{+/-}$ intercrosses and comparing *Egfl7*$^{-/-}$ tissues with littermate controls. To exclude maternal contribution of a wild-type *Egfl7* allele to the placenta of *Egfl7*$^{-/-}$ conceptuses, we performed all subsequent studies using *Egfl7*$^{-/-}$ intercrosses. *Egfl7*$^{-/-}$ mice from *Egfl7*$^{+/-}$ intercrosses were viable and born at the expected Mendelian ratio, demonstrating that abrogation of Egfl7 does not compromise embryonic viability; however, crown-to-rump lengths of *Egfl7*$^{-/-}$ embryos at late gestation were significantly decreased (19.4±1.6 mm versus 17.7±0.4 mm) (Fig. 2N). We next measured crown-to-rump lengths from control C57BL/6J×C57BL/6J (+/+) and *Egfl7*$^{-/-}$ ×*Egfl7*$^{-/-}$ matings at E9.5, E12.5 and E18.5. Loss of *Egfl7* did not affect crown-to-rump lengths at E9.5 (2.05±0.2 mm versus 1.92 ±0.3 mm) (Fig. 2A,B,E), the stage when Egfl7 expression peaks in the embryo (Fitch et al., 2004). By contrast, the lengths of *Egfl7*$^{-/-}$ embryos were approximately 1 mm shorter than C57BL/6J control embryos at E12.5 (9.15±0.8 mm versus 8.08±0.7 mm) (Fig. 2C-E), when Egfl7 expression in the placenta peaks (Lacko et al., 2014). Significant growth restriction of *Egfl7*$^{-/-}$ embryos was observed up to the final stages of gestation, at E18.5 (20.79±1.8 mm versus 18.80 ±1.4 mm) (Fig. S1A-C). To determine whether *Egfl7* loss of function results in vascular patterning defects in the embryo, immunofluorescent staining was performed on sections of E9.5 and E12.5 embryos from C57BL/6J and *Egfl7*$^{-/-}$ mice using the pan-endothelial marker CD31. No gross vascular defects or developmental delays were observed in *Egfl7*$^{-/-}$ embryos at either

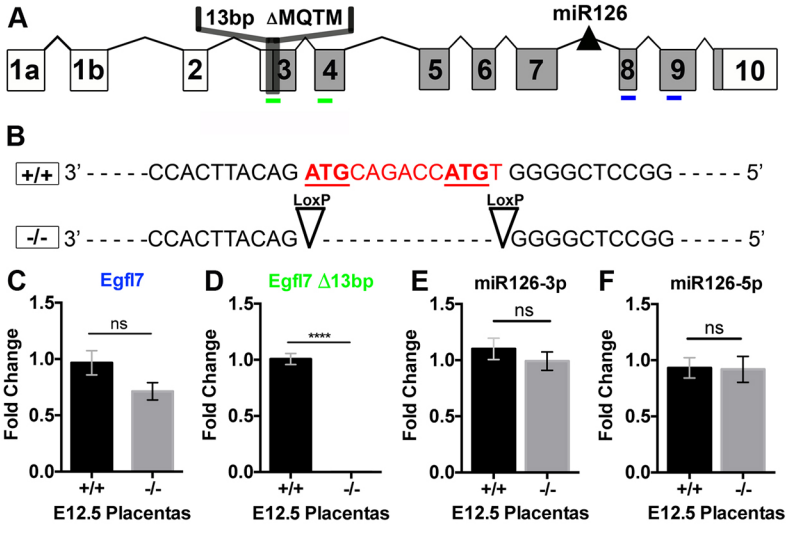

Fig. 1. Generation of *Egfl7* loss-of-function mice. (A) Schematic representation of the *Egfl7* gene structure. Shaded regions represent protein-coding exons. The positions of the microRNA miR-126 and the 13 bp deletion in the mutant *Egfl7* allele are depicted (not drawn to scale). Locations of primer sets are demarcated in blue (C) and green (D). (B) Sequence of the wild type (+/+) and modified (–/–) *Egfl7* allele. The 13 bp deleted sequence is depicted in red with the two putative translational start sites underlined. (C,D) Real time RT-PCR for unmodified Egfl7 mRNA (C) and modified Egfl7 mRNA containing the 13 bp deletion (D) in E12.5 placentas from C57BL/6J (+/+, *n*=6) and *Egfl7*$^{-/-}$ mice (–/–, *n*=5). (E,F) Real time RT-PCR for miR126-3p (E) and miR126-5p (F) in E12.5 placentas from C57BL/6J (+/+, *n*=3) and *Egfl7*$^{-/-}$ (–/–, *n*=3) mice showing no change in miR-126 expression. Student's *t*-test; data are mean ±s.e.m. ****P<0.0001.

Development (2017) 144, 2469-2479 doi:10.1242/dev.147025

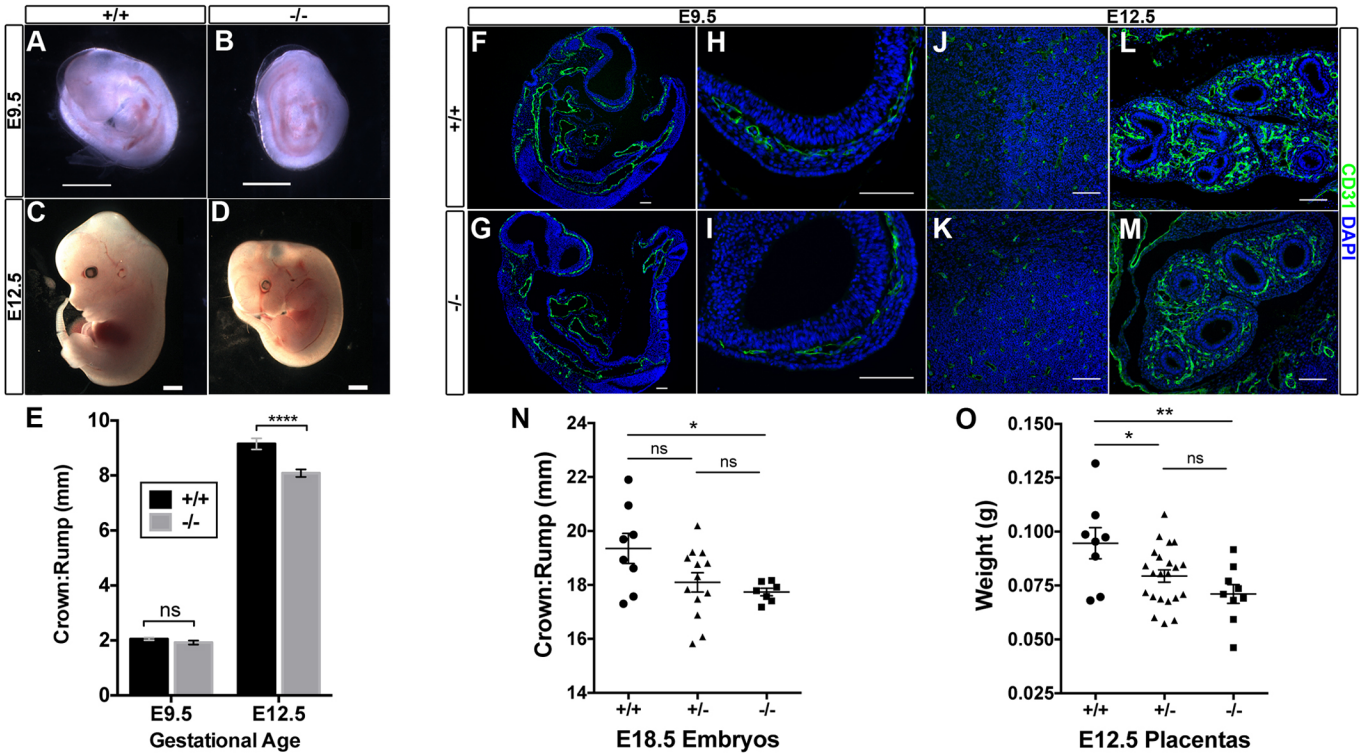

Fig. 2. *Egfl7* loss of function results in reduced placental weight and fetal growth restriction. (A-D) Representative images of E9.5 (A,B) and E12.5 (C,D) C57BL/6J and *Egfl7*$^{-/-}$ embryos. (E) Quantification of the crown-to-rump lengths of E9.5 (+/+, *n*=23; –/–, *n*=21) and E12.5 (+/+, *n*=18; –/–, *n*=23) embryos showing a significant reduction in *Egfl7*$^{-/-}$ embryo lengths at E12.5, but not at E9.5 (Student's *t*-test). (F-M) Immunofluorescent staining for CD31 (green) and DAPI (blue) on sections of E9.5 and E12.5 C57BL/6J (+/+, F,H,J,L) and *Egfl7*$^{-/-}$ (G,I,K,M) embryos depicting no gross vascular defects. (F,G) Cross-section of whole E9.5 embryos. High-magnification images of the head vasculature at E9.5 (H,I) and E12.5 (J,K), and of the developing lung bud vasculature (L,M). (N) Quantification of the crown-to-rump lengths from *Egfl7*$^{+/-}$ intercrosses showing a significant reduction in *Egfl7*$^{-/-}$ embryo lengths at E18.5. (O) E12.5 placenta weights from *Egfl7*$^{+/-}$ intercrosses demonstrating a significant decrease in *Egfl7*$^{+/-}$ and *Egfl7*$^{-/-}$ placentas. Data are mean±s.e.m. One-way ANOVA, Tukey's multiple comparison test. **P*<0.05, ***P*<0.01, *****P*<0.0001. ns, not significant. Scale bars: 1 mm in A-D; 100 µm in F-M. See also Fig. S1.

stage examined, including the vasculature of the developing head, heart, aorta, lung buds and intersomitic vessels (Fig. 2F-M; Fig. S1D-K), consistent with recently published studies in a different *Egfl7* specific knockout mouse model (Kuhnert et al., 2008). Taken together, these results reveal a significant growth restriction of *Egfl7*$^{-/-}$ embryos after the onset of placenta development, suggesting placental insufficiencies as a possible cause of IUGR.

IUGR was first observed at E12.5, the developmental stage when the three layers of the mature placenta have formed and placental Egfl7 expression peaks, and continued to E18.5 (Fig. 2E, Fig. S1C). Strikingly, growth restriction at E12.5 coincided with a significant decrease in total weight of *Egfl7*$^{+/-}$ and *Egfl7*$^{-/-}$ placentas from *Egfl7*$^{+/-}$ intercrosses (+/+ 0.0946±0.02 g versus +/– 0.0794±0.01 g versus –/– 0.0711±0.01 g) (Fig. 2O). As growth restriction was also observed for *Egfl7*$^{+/-}$ and *Egfl7*$^{-/-}$ embryos (Fig. 2N), and similar weights were observed for male and female *Egfl7*$^{+/-}$ placentas from *Egfl7*$^{+/-}$ intercrosses when examined by PCR for Sry and Jarid (Fig. S1N), we can rule out predominant maternal effects or sexual dimorphism as the cause for the *in vivo* phenotype. Thus, our data demonstrate that *Egfl7* plays an important role in placental growth, and indicate that placental defects may underlie the observed growth restriction in *Egfl7*$^{-/-}$ mutant embryos.

Egfl7$^{-/-}$ placentas exhibit vascular patterning defects and reduced fetal blood space in the labyrinth

To further investigate placental insufficiencies in mice with *Egfl7* loss of function, we examined the morphology of *Egfl7*$^{-/-}$ and control placentas. Paraffin wax-embedded E12.5 *Egfl7*$^{+/+}$ and *Egfl7*$^{-/-}$ placentas from *Egfl7*$^{+/-}$ intercrosses were sectioned, and placental morphology was assayed after Hematoxylin and Eosin staining (Fig. 3A-D). All three placental layers, including the maternal decidua, junctional zone and fetal labyrinth, formed in both *Egfl7*$^{-/-}$ and control placentas (Fig. 3A,B). Strikingly, at high magnification, the fetal labyrinth of *Egfl7*$^{-/-}$ placentas exhibited marked vascular patterning defects when compared with control placentas (Fig. 3C,D), whereas the maternal decidua and junctional zone showed no abnormalities (Fig. S1L,M). The maternal and fetal blood spaces are easily distinguished, as fetal vessels contain nucleated embryonic erythrocytes. A well-patterned fetal capillary network was revealed in the control placentas, consisting of open, lumenized, patent vessels adjacent to maternal lacunae, and separated by a thin layer of trophoblasts and ECs (Fig. 3C). In contrast, the fetal vessels in *Egfl7*$^{-/-}$ placentas were narrowed and markedly constricted (Fig. 3D). The reduced fetal blood space area resulted in accumulation of erythrocytes within the constricted blood vessels.

We next characterized the mutant phenotype of *Egfl7*$^{-/-}$ placentas by immunofluorescence analysis. Cryosections of C57BL/6J and *Egfl7*$^{-/-}$ placentas from E12.5 conceptuses were assayed for expression of the endothelial marker CD31 and the pan-trophoblast marker cytokeratin. In *Egfl7*$^{-/-}$ placentas, ECs surround the irregularly patterned and narrowed fetal capillaries, whereas trophoblast cells lining the maternal blood spaces showed no obvious patterning defects (Fig. 3E-J). Quantification of the area of

Development (2017) 144, 2469-2479 doi:10.1242/dev.147025

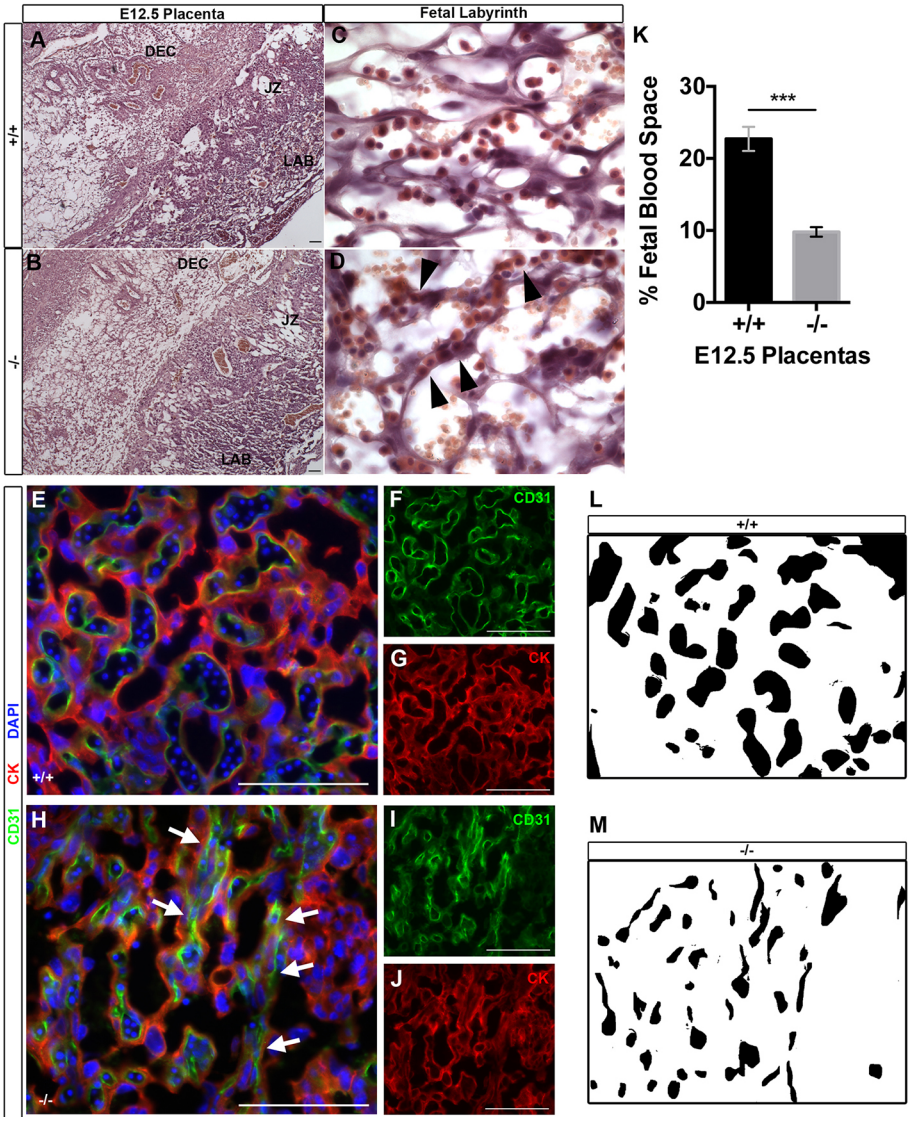

Fig. 3. Vascular patterning defects and reduced fetal blood space in the fetal labyrinth of *Egfl7*$^{-/-}$ placentas. (A-D) Hematoxylin and Eosin-stained sections of E12.5 C57BL/6J (+/+) (A,C) and *Egfl7*$^{-/-}$ (B,D) placentas. (A,B) Low-magnification images depicting formation of three major placental layers: fetal labyrinth (LAB), junctional zone (JZ) and maternal decidua (DEC). (C,D) High-magnification images of the fetal labyrinth depicting narrowed fetal capillary space in *Egfl7*$^{-/-}$ placentas (arrowheads). (E-J) Double immunofluorescence staining for the pan-endothelial marker CD31 (green; F,I), the pan-trophoblast marker cytokeratin (red; G,J) and nuclear DAPI (blue; E,H) on placenta sections from E12.5 C57BL/6J (+/+; E-G) and *Egfl7*$^{-/-}$ (–/–; H-J) mice. High magnification of the fetal labyrinth zone is shown (E,H). Arrows mark narrowed fetal capillary spaces. (K) Quantification of the area of fetal blood space in the fetal labyrinth of C57BL/6J (+/+, *n*=3 placentas) and *Egfl7*$^{-/-}$ (–/–, *n*=3 placentas) mice from (E,H). (L,M) Representative images of fetal blood space area quantification demonstrating a significant decrease in the percentage of area covered by fetal capillaries in the fetal labyrinth zone of *Egfl7*$^{-/-}$ placentas (M). Student's *t*-test; data are mean±s.e.m. ***P<0.001. Scale bars: 100 µm. See also Fig. S1.

fetal capillary lumens revealed a significant reduction in fetal capillary blood space in the labyrinth of *Egfl7*$^{-/-}$ placentas (22.7± 5.0% versus 9.8±2.0%) (Fig. 3K-M). Taken together, our histological and immunofluorescence analyses reveal that *Egfl7* loss of function results in abnormal vascular patterning and reduced fetal blood space of the placental fetal labyrinth.

Egfl7$^{-/-}$ conceptuses show reduced chorioallantoic branching morphogenesis

Formation of the placenta and the fetal labyrinth begins at E8.5 when the allantoic mesoderm comes into contact with a flat chorion and initiates invaginations of the chorionic plate. Allantoic ECs then invade into the folds of chorionic trophoblasts and subsequently undergo branching morphogenesis to form the extensive vascular network of the fetal labyrinth (Rossant and Cross, 2001). Notably, Egfl7 is highly expressed by the allantois (Bambino et al., 2014). We next investigated whether *Egfl7*$^{-/-}$ placentas exhibit defects in chorioallantoic branching morphogenesis at this initial stage of placental development. To visualize chorioallantoic attachment in conceptuses at E8.5, we generated 100 µm vibratome sections of whole conceptuses (Fig. 4A,B). Results revealed that *Egfl7*$^{-/-}$ conceptuses contained a smaller allantois, which less efficiently covered the flat chorion when compared with stage-matched controls. Furthermore, *Egfl7*$^{-/-}$ allantoises did not exhibit the characteristic funnel-like shape seen in controls (Fig. 4A-D, Movies 1, 2). Quantification of the percentage of chorion covered by the attached allantois revealed *Egfl7*$^{-/-}$ allantoises covered 20% less of the chorion at E8.5 than controls (62.9±5.3% versus 42.3±13.5%) (Fig. 4E).

To visualize chorionic invaginations, immunofluorescent staining for CD31 and cytokeratin was performed on 100 µm vibratome sections of E8.5 and E9.5 conceptuses from C57BL/6J and stage-matched *Egfl7*$^{-/-}$ mice. Quantification of the number of invaginations and length of invaginations of the invading ECs into the chorion was performed on confocal *z*-stack images. *Egfl7*$^{-/-}$ placentas displayed significantly fewer (11.3±1.5 versus 7.3±0.6) and shorter (0.30±0.02 mm versus 0.13±0.01 mm) invaginations than control placentas (Fig. 4F-I, Movies 3, 4). Cryosections of C57BL/6J and *Egfl7*$^{-/-}$ whole conceptuses were stained for CD31 and cytokeratin to analyze cellular detail of the invading blood vessels (Fig. 4J-K). *Egfl7*$^{-/-}$ invaginations were lined with CD31-positive ECs, but were stunted, widened and less organized when compared with controls. Thus, *Egfl7*$^{-/-}$ conceptuses display defects in branching morphogenesis at the initial stages of placental development.

Development (2017) 144, 2469-2479 doi:10.1242/dev.147025

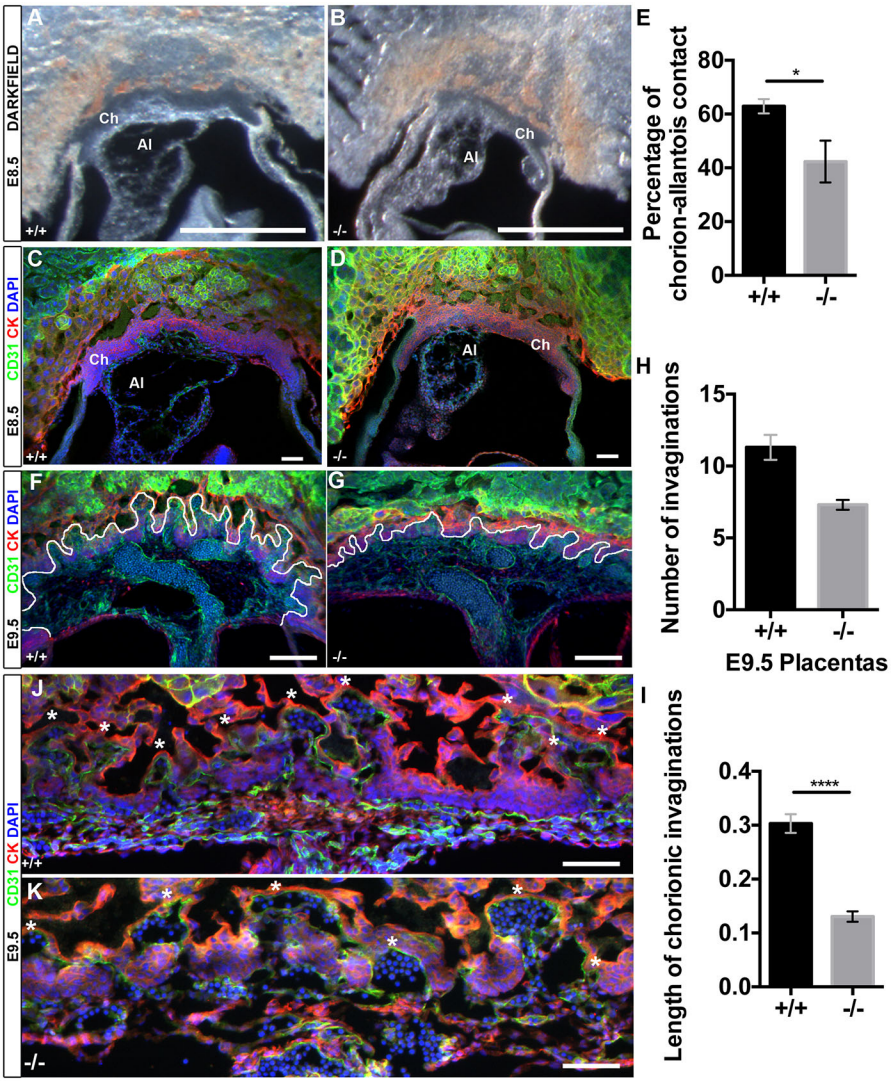

Fig. 4. *Egfl7*$^{-/-}$ conceptuses show reduced chorioallantoic branching morphogenesis. (A,B) Representative dark-field images of 100 µm vibratome sections of E8.5 conceptuses from C57BL/6J (+/+) and *Egfl7*$^{-/-}$ mice. (C,D) Confocal images of 100 µm vibratome sections of E8.5 conceptuses from C57BL/6J (+/+) and *Egfl7*$^{-/-}$ mice, immunostained for CD31 (green), cytokeratin (red) and nuclear DAPI (blue), demonstrating a small allantois less efficiently adhered to the chorion in the mutants. (E) Quantification of the percentage of chorion that is attached to the allantois revealing a significant decrease in chorio-allantoic contact in *Egfl7*$^{-/-}$ conceptuses (+/+, *n*=5; –/–, *n*=4). (F,G) Confocal images of 100 µm vibratome sections of E9.5 conceptuses from C57BL/6J (+/+) and *Egfl7*$^{-/-}$ mice, immunostained for CD31 (green), cytokeratin (red) and DAPI (blue). Chorionic invaginations into which fetal vasculature is invading are indicated by a white line. (H,I) Quantification of the number (H) and length in mm (I) of invaginations in E9.5 placentas of C57BL/6J (+/+, *n*=3) and *Egfl7*$^{-/-}$ (*n*=3) mice. (J,K) High-magnification images of 10 µm cryosections of E9.5 placentas showing stunted and reduced number of invaginations in *Egfl7* mutant placentas (K). Asterisks indicate each chorionic fold. Ch, chorion; Al, allantois. Student's *t*-test; data are mean±s.e.m. **P*<0.05, *****P*<0.0001. Scale bars: 500 µm in A,B; 100 µm in C,D,J,K; 200 µm in F,G.

Egfl7$^{-/-}$ placental endothelial cells exhibit defects in cell migration, sprouting and branching morphogenesis

To determine whether defects in EC function underlie the vascular phenotype observed in *Egfl7* loss-of-function mutant placentas, we performed functional analyses of primary ECs isolated from *Egfl7*$^{-/-}$ and control placentas. Primary placental ECs were isolated from midgestation C57BL/6J and *Egfl7*$^{-/-}$ placentas, and long-term placental EC cultures were established by infection with lentivirus expressing myristolated Akt, as previously described (Kobayashi et al., 2010; Poulos et al., 2015). Immunostaining for the endothelial markers CD31, Vecad and Erg, as well as for the trophoblast marker cytokeratin revealed that these cultures contained >99% ECs (Fig. S2A-F).

To examine migration of placental ECs, we performed a scratch wound healing assay, as previously described (Liang et al., 2007). A scratch wound was created in confluent monolayers of control and *Egfl7*$^{-/-}$ placental ECs, and cell migration was assayed by image analyses at 0 h and 24 h. *Egfl7*$^{-/-}$ placental ECs were significantly slower in migrating towards, and closing, the scratch wound at 24 h (Fig. 5A-E). The observed defect in wound closure was not due to changes in cell proliferation or apoptosis, as the percentage of Ki67-positive cells at 24 h and rates of proliferation in *Egfl7*$^{-/-}$ and control placental ECs were similar (Fig. S2G-J), and less than 0.5% caspase 3-positive cells were observed in either cell type (not shown). Consistent with these results, no significant difference in the number and percentage of proliferating endothelial and non-endothelial cells was observed between *Egfl7*$^{-/-}$ and C57BL/6J placentas *in vivo*, as determined by intraperitoneal injection of EdU and subsequent immunostaining for CD31, Erg and cytokeratin (Fig. S3).

To determine whether Egfl7 plays a role in placental EC sprouting, we performed a fibrin gel bead assay, an *in vitro* model that recapitulates key early stages of new vessel formation in a three-dimensional matrix, including vessel sprouting and maturation (Nehls and Drenckhahn, 1995; Tattersall et al., 2016; Nakatsu and Hughes, 2008). *Egfl7*$^{-/-}$ placental ECs formed significantly fewer and shorter endothelial sprouts when compared with control placental ECs at day 2 and day 4 in culture (Fig. 5F-K).

Finally, we assayed the ability of the placental ECs to form a capillary-like network using a cord formation assay (Kubota et al., 1988; Arnaoutova and Kleinman, 2010). Control and *Egfl7*$^{-/-}$ placental ECs were plated on growth factor reduced matrigel, and imaged after 2 h and 4 h. Control placental ECs formed a honeycomb-like network of connected EC cords beginning at 2 h and stabilizing at 4 h. In contrast, *Egfl7*$^{-/-}$ placental ECs completely failed to form a network of vascular cords and instead exhibited cellular clusters with fewer nodes or connections (Fig. 5L-O). Quantification of cord formation at 4 h showed a significant

Development (2017) 144, 2469-2479 doi:10.1242/dev.147025

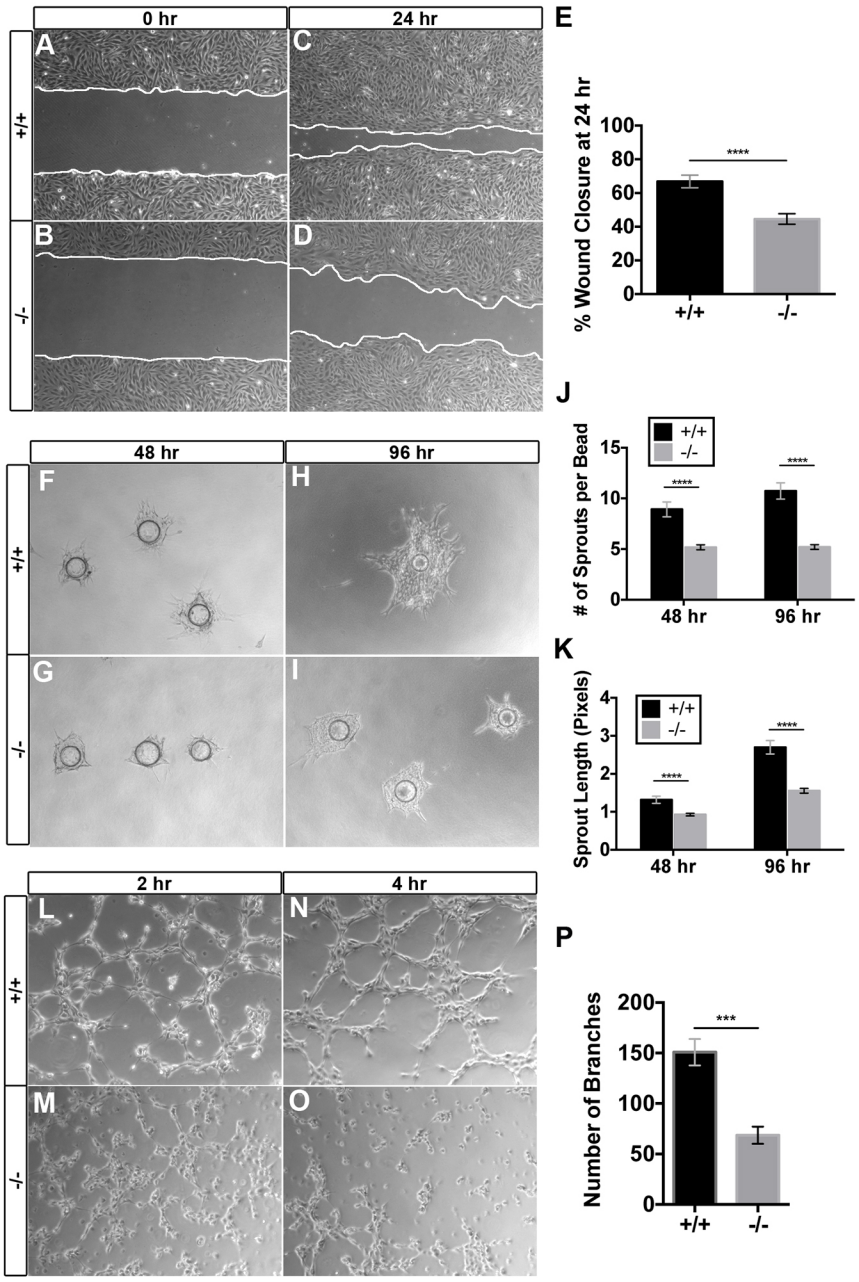

Fig. 5. *Egfl7*$^{-/-}$ placental endothelial cells exhibit defects in cell migration, sprouting and branching morphogenesis. Isolated placental endothelial cells (ECs) from C57BL/6J (+/+) and *Egfl7*$^{-/-}$ mice were used for functional assays *in vitro*. (A-D) Representative images of the placental ECs from the scratch-wound assay. Collective EC migration was observed at 24 h (C,D). White lines indicate the leading edge of migrating cells. (E) Quantification of the percentage of wound area closed at 24 h (+/+, *n*=18; –/–, *n*=18). (F-I) Representative images of C57BL/6J (+/+) and *Egfl7*$^{-/-}$ placental ECs subjected to a bead sprouting assay, imaged at 48 h (F,G) and 96 h (H,I). (J,K) Quantification of the number of sprouts per bead (J) and the total sprout length (K) (+/+, *n*=11-12; –/–, *n*=20-23). (L-O) Representative images of C57BL/6J (+/+) and *Egfl7*$^{-/-}$ placental ECs subjected to a cord formation assay. Formation of cord-like structures on matrigel was observed at 2 h (L,M) and 4 h (N,O). (P) Quantification of the number of branches observed at 4 h, demonstrating a significant decrease in cord formation in *Egfl7*$^{-/-}$ placental ECs (+/+, *n*=20; –/–, *n*=15). Student's *t*-test; data are mean±s.e.m. ***P<0.001, ****P<0.0001. See also Figs. S2 and S4.

decrease in the number of branches (Fig. 5P). In contrast to the placental ECs, primary Akt-activated ECs from E10.5 C57BL/6J and *Egfl7*$^{-/-}$ embryos did not show a significant difference in cell migration or proliferation (Fig. S4).

Our functional analyses of *Egfl7*$^{-/-}$ ECs have uncovered defects in placental EC function that are consistent with abnormal vascular patterning. Notably, these results corroborate the *in vivo* data showing an irregularly formed fetal vascular network in the placentas of *Egfl7*$^{-/-}$ mice.

Egfl7 knockout results in dysregulation of genes associated with chorioallantoic branching morphogenesis and in downregulation of the extracellular matrix protein Mmrn1

To elucidate the molecular mechanism by which Egfl7 regulates placental vascular development, we used a candidate gene approach. We first examined whether genes known to regulate chorioallantoic branching morphogenesis are dysregulated in *Egfl7*$^{-/-}$ mutants, given that *Egfl7*$^{-/-}$ placentas exhibit defects in this initial step of placental development. Specifically, we analyzed the expression of Gcm1, a transcription factor that is crucial for the initiation and maintenance of branching morphogenesis in the developing placenta. *Gcm1* mutant mice display a complete block in chorioallantoic branching (Anson-Cartwright et al., 2000). Real time RT-PCR analysis was performed on C57BL/6J and *Egfl7*$^{-/-}$ pre-placental tissues (chorion, ectoplacental cone and decidua) isolated from E8.5 conceptuses and from placentas at E9.5 and E12.5. Results showed Gcm1 transcript levels were significantly reduced in *Egfl7*$^{-/-}$ mutants at E8.5 and E9.5. At E12.5, Gcm1 levels were reduced without reaching significance (Fig. 6A). Immunohistochemistry for Gcm1 on E9.5 cryosections of C57BL/6J and *Egfl7*$^{-/-}$ placentas revealed that Gcm1 protein localized in the nucleus and cytoplasm of trophoblasts at and between chorionic invaginations, and was reduced in *Egfl7*-null placentas (Fig. 6E-J).

Development (2017) 144, 2469-2479 doi:10.1242/dev.147025

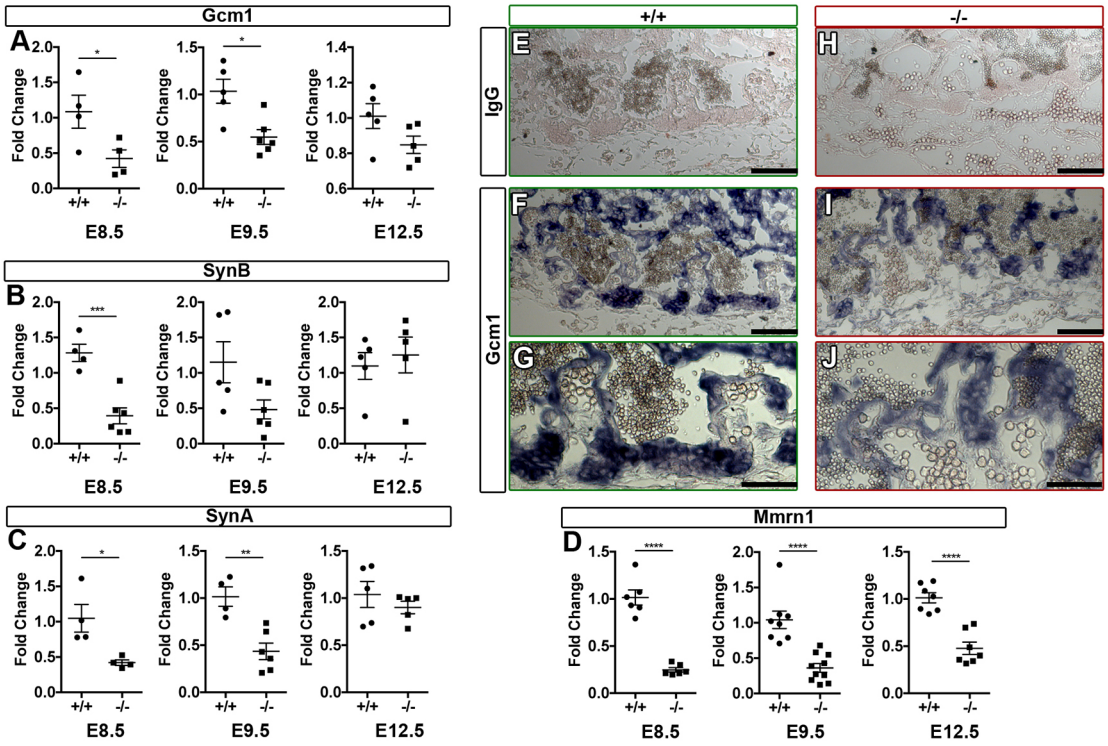

Fig. 6. *Egfl7* knockout results in dysregulation of genes associated with chorioallantoic branching morphogenesis and downregulation of the extracellular matrix gene *Mmrn1*. Real time RT-PCR for Gcm1 (A), Synb (B), Syna (C) and Mmrn1 (D) on pre-placental tissues (E8.5; chorion, ectoplacental cone and decidua) and placentas (E9.5, E12.5) from C57BL/6J (+/+, *n*=4-6) and *Egfl7*$^{-/-}$ (*n*=4-6) mice. Results demonstrate a significant decrease in gene expression for *Gcm1* and *Syna* at E8.5 and E9.5, *Synb* at E8.5, and extracellular matrix gene *Mmrn1* at all stages. Student's *t*-test; data are mean ±s.e.m. **P*<0.05, ***P*<0.01, ****P*<0.001, *****P*<0.0001. (E-J) Immunohistochemistry on E9.5 sections of C57BL/6J (+/+) and *Egfl7*$^{-/-}$ placentas for Gcm1 (purple precipitate) showing altered expression in *Egfl7*-null placentas. (E,H) IgG control staining for antibody specificity. (F,G,I,J) Gcm1 localization to chorionic invaginations. Scale bars: 100 µm in E,F,H,I; 50 µm in G,J. See also Figs. S5-8.

To further establish that Gcm1 signaling is dysregulated in Egfl7 loss-of-function placentas, we assayed for expression of the Gcm1 target gene *Synb*, which encodes an endogenous retrovirus envelope protein that plays a role in trophoblast fusion (Dupressoir et al., 2005, 2011). A concomitant significant decrease was observed for Synb transcript levels in *Egfl7*$^{-/-}$ pre-placental tissues at E8.5, while no significant difference was observed in E9.5 or E12.5 placentas (Fig. 6B). Notably, mice with a deletion in another endogenous retroviral envelope gene that is important for trophoblast development, *Syna*, display significantly reduced fetal blood space (Dupressoir et al., 2009). Syna expression was significantly decreased in *Egfl7*$^{-/-}$ pre-placental tissues at E8.5 and placentas at E9.5, and was unchanged at E12.5 (Fig. 6C). In contrast, no significant differences in expression of Itga4 and Vcam1, two key cell-adhesion molecules that are important for chorioallantoic attachment, were detected at E8.5, E9.5 or E12.5 (Fig. S8). Together, these results reveal that crucial regulatory genes involved in chorioallantoic branching morphogenesis are dysregulated early in *Egfl7*$^{-/-}$ placentas, which provides a molecular mechanism for the observed defects at the onset of placental development.

Previous studies have shown that Egfl7 modulates Notch signaling *in vivo* in mouse embryos and *in vitro* in HUVECs, human trophoblast cells and neural stem cells (Nichol et al., 2010; Massimiani et al., 2015; Schmidt et al., 2009). To examine whether Egfl7 modulates Notch signaling in the developing placental labyrinth, we performed real time RT-PCR for Notch target genes in pre-placental tissues (E8.5) or placentas (E9.5, E12.5) from C57BL/6J control and *Egfl7*$^{-/-}$ mice. Hey2 transcript levels were significantly reduced in E12.5 *Egfl7*$^{-/-}$ placentas when compared with C57BL/6J controls, and were unchanged at E8.5 and E9.5 (Fig. S5B). No significant difference was observed in mRNA levels of Notch target genes Hey1 and Hes1 in *Egfl7*$^{-/-}$ tissues at E8.5, E9.5 or E12.5 (Fig. S5A,C).

A recent study demonstrated compensatory roles for Emilin family genes (*emilin3a*, *emilin3b* and *emilin2a*) in *egfl7* mutant zebrafish (Rossi et al., 2015). To determine whether *Egfl7* loss of function in mice similarly results in changes in Emilin family gene expression, we performed real time RT-PCR for Emilin1, Emilin2, Emilin3, Mmrn1 and Mmrn2 on mouse pre-placental tissues, placentas and embryos from C57BL/6J and *Egfl7*$^{-/-}$ mice. Results of these experiments revealed that Mmrn1 mRNA was significantly downregulated in *Egfl7*$^{-/-}$ pre-placentas at E8.5, and in placentas at E9.5 and E12.5 (Fig. 6D). Mmrn1 was the only Emilin family member that was dysregulated in extra-embryonic tissues at all stages examined. A small but significant decrease in expression of Mmrn2 and Emilin1 was found in *Egfl7*$^{-/-}$ placentas at E9.5 (Fig. S6B). Overall expression of Emilin3 was very low at all stages examined; however, a significant reduction was observed at E8.5 (Fig. S6A). No significant difference in expression of other Emilin family members (Emilin1, Emilin2, Emilin3 and Mmrn2) was detected at all other stages (Fig. S6). Furthermore, no significant changes were detected in Emilin family genes in *Egfl7*$^{-/-}$ mutant embryos at E9.5 and E12.5 (Fig. S7). In contrast to studies in zebrafish embryos, compensation by Emilin family genes was not observed in *Egfl7*$^{-/-}$ embryos or placentas.

To investigate whether a global reduction in gene expression is detected in *Egfl7*$^{-/-}$ placentas, we performed real time RT-PCR on two additional genes with differing roles in placentation, *Hand1* and

Development (2017) 144, 2469-2479 doi:10.1242/dev.147025

Vecad (*Cdh5* – Mouse Genome Informatics) and found no significant difference in their expression at E8.5, E9.5 or E12.5 (Fig. S8D-F). Taken together, we have uncovered that dysregulation of specific genes, *Gcm1*, *Syna*, *Synb* and *Mmrn1*, underlies the observed defects in branching morphogenesis and labyrinth formation.

Altered vascular patterning results in reduced feto-placental perfusion in *Egfl7*$^{-/-}$ placentas

The aberrant vascular patterning and narrowed fetal capillary blood space observed in *Egfl7*$^{-/-}$ placentas raised the possibility that blood perfusion of the mutant placentas was compromised. To test this, we performed microangiography in control and *Egfl7*$^{-/-}$ conceptuses isolated at E12.5, and analyzed the three-dimensional architecture of the placental vasculature. In brief, whole E12.5 conceptuses were injected with a tomato-lectin solution into the umbilical artery to mark the blood-conducting vessels in the fetal labyrinth. Perfusion was restricted to the fetal labyrinth zone of the placenta. Analyses of 100 µm sections of C57BL/6J control placentas revealed a dense arborized vascular network of blood-conducting vessels in the fetal labyrinth (Fig. 7A,C-E). Large chorionic vessels at the base of the placentas branched into smaller vessels of the fetal labyrinth, and further into the dense capillary network in order to cover a large surface area (Fig. 7A). In contrast, *Egfl7*$^{-/-}$ placentas exhibited locally restricted and reduced feto-placental perfusion. The large chorionic vessels were well perfused. However, only sporadic areas with well-perfused, smaller branched vessels surrounded by areas of poorly perfused vessels were observed in *Egfl7*$^{-/-}$ placentas (Fig. 7B,F-H).

To determine whether reduced conduction of blood results from constricted fetal capillaries lined by ECs and from vascular patterning defects, we performed retrospective immunofluorescence staining for CD31 on vibratome sections of placentas post-microangiography. Confocal imaging of the fetal labyrinth revealed a well-patterned perfused fetal capillary network lined by CD31-positive ECs with a smooth cell surface in C57BL/6J control placentas (Fig. 7C-E). In contrast, *Egfl7*$^{-/-}$ fetal labyrinth capillaries were tortuous, and their organization was markedly perturbed (Fig. 7F-H). A subset of these vessels was poorly perfused. Strikingly, results of these analyses revealed that sites of poor perfusion localized to small, narrowed or constricted fetal capillaries in *Egfl7*$^{-/-}$ placentas (Fig. 7F-H, Movies 5, 6). Together, our results show that *Egfl7* loss of function results in abnormal vascular patterning of the fetal labyrinth, EC dysfunction and reduced feto-placental perfusion at sites of constricted fetal capillaries, all of which underlie intrauterine growth restriction.

DISCUSSION

Despite the crucial importance of the placenta for proper mammalian development, a complete understanding of the precise molecular pathways that are responsible for placental development and homeostasis remains largely elusive. However, considerable progress has been made through studying single gene mutations in mice (Rossant and Cross, 2001; Watson and Cross, 2005). Here, we show for the first time that *Egfl7* is crucial for placental vascular development and embryonic growth. EGFL7 is a secreted, largely endothelial-restricted angiogenic factor that is associated with the extracellular matrix. We have generated a novel mouse model with loss of a functional *Egfl7* gene, while fully maintaining expression of the intronic miR-126. The targeted allele in this study contains a deletion of the two translational start sites in exon 3, whereas the mutant allele described in a previous *Egfl7* loss-of-function study deleted exons 5-7, leaving the start codons intact (Kuhnert et al., 2008). Our study firmly establishes that knockout of *Egfl7* in mice

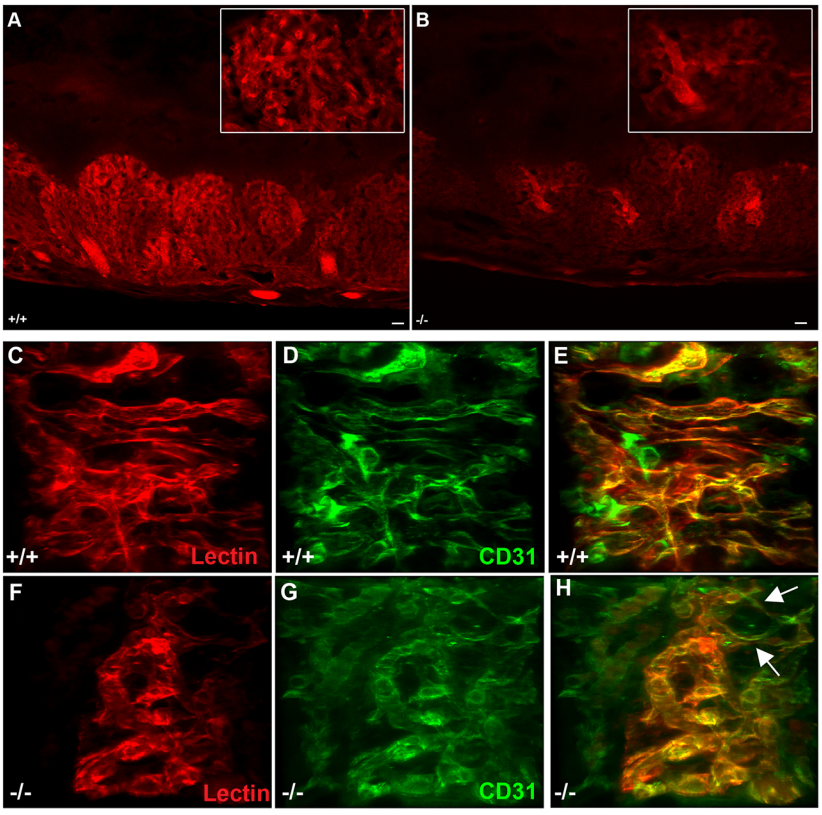

Fig. 7. Altered vascular patterning results in reduced feto-placental perfusion at sites of constricted fetal capillaries in *Egfl7*$^{-/-}$ placentas. Microangiography of placentas from E12.5 C57BL/6J and *Egfl7*$^{-/-}$ mice was performed using tomato-lectin (red). Representative images of 100 µm vibratome cross-sections of E12.5 placentas from C57BL/6J (+/+; A) and *Egfl7*$^{-/-}$ (B) mice. Insets: higher magnification of representative images showing areas of reduced feto-placental perfusion in *Egfl7*$^{-/-}$ mice. (C-H) Three-dimensional reconstruction of *z*-stack confocal images of placentas perfused with tomato-lectin (red) and subsequently immunostained with CD31 (green). Arrows indicate narrowed fetal capillaries and areas where a reduction in perfusion begins. Scale bars: 100 µm in A,B.

Development (2017) 144, 2469-2479 doi:10.1242/dev.147025

results in abnormal chorioallantoic branching morphogenesis and vascular patterning of the fetal labyrinth, EC dysfunction and reduced feto-placental perfusion at sites of constricted fetal capillaries, all of which underlie IUGR.

The mutant phenotypes in *Egfl7*$^{-/-}$ placentas appear to be specific to the formation and patterning of the fetal labyrinth endothelium. In support of this, cultured placental, but not embryonic, ECs require Egfl7 for proper cell migration, sprouting and cord formation, suggesting that the primary defect is in ECs of the placenta. Furthermore, our studies indicate that maternal effects or sexual dimorphism do not contribute to the *in vivo* phenotype. Of note, we have recently reported novel sites of Egfl7 expression in junctional zone placental trophoblasts in mice and in cytotrophoblasts and syncytiotrophoblasts in human placentas, in addition to its expression in the fetal and maternal placental endothelium (Lacko et al., 2014). In fact, EGFL7 in human cultured trophoblast cells promotes migration and invasion through activation of NOTCH and EGFR signaling pathways (Massimiani et al., 2015). Future studies using trophoblast-specific knockout or knockdown of Egfl7 will address the possibility of non-cell autonomous and non-endothelial effects on branching morphogenesis in the labyrinth.

One striking result of our studies was the detection of vascular defects in the fetal labyrinth, and the lack of an overt phenotype in the embryonic or the adult vasculature. This could be explained by the developmental origin and/or the microenvironment of the ECs. The labyrinth EC lineage is derived from the extra-embryonic mesoderm of the allantois, whereas all embryonic and adult ECs are derived from the mesoderm of the embryo proper. In support of this, the transcriptome of placental ECs is distinct from that of ECs isolated from any other organ (Nolan et al., 2013) (J.M.B., unpublished). Furthermore, the labyrinth endothelium likely receives unique signals from its microenvironment, including trophoblast cells that are restricted to the placenta. Finally, previous studies have suggested a role for Egfl7 in the endothelium specifically during physiological stress, such as vascular injury (Campagnolo et al., 2005; Bambino et al., 2014). It is conceivable that pregnancy exposes the placental vasculature to similar stress-like challenges, resulting in placental insufficiencies in *Egfl7*$^{-/-}$ females.

The placental defects, together with the dysregulation of key pathway genes, are consistent with Egfl7 acting in both a paracrine and autocrine manner. During early stages of placental development, between E8.5 and E9.5, Egfl7 is prominently expressed in angiogenic progenitors and the emerging endothelium of the allantois (Bambino et al., 2014). Loss of *Egfl7* results in defects in chorioallantoic attachment and branching morphogenesis, concomitant with significantly reduced expression of the key trophoblast-specific transcriptional regulator genes *Gcm1*, *Synb*, and *Syna*. Rescue experiments would be needed to verify that their decreased expression is the cause of the mutant branching phenotype. Interestingly, defects in chorionic branching morphogenesis are the leading cause of midgestation embryonic lethality in the mouse (Rossant and Cross, 2001). Our results suggest that allantois-derived EGFL7 is a crucial signaling factor specifically for branching morphogenesis and during early vascular development in the placenta, but not in the embryo. Importantly, allantois explants co-cultured with trophoblasts indicate that signals originating from the allantois initiate branching morphogenesis and induction of Gcm1 expression in the chorion (Cross et al., 2006; Downs and Gardner, 1995). Our results implicate the allantois-derived secreted EGFL7 to be such a paracrine signal.

The vascular patterning phenotype observed in *Egfl7*$^{-/-}$ placentas *in vivo* and in cultured placental ECs *in vitro* could be explained by an autocrine role of Egfl7, and may involve a poorly maintained extracellular matrix (ECM) structure. Previously, Egfl7 was reported to promote proangiogenic functions by inhibiting the formation of elastic fibers, thus reducing rigidity and influencing EC behavior through signaling to the ECM (Lelièvre et al., 2008). Members of the Emilin protein family (Emilin1, Emilin2, Emilin3, Mmrn1 and Mmrn2) are located predominantly in the ECM, are proangiogenic, and have been shown to modulate arterial blood pressure, elastogenesis and platelet hemostasis (Braghetta et al., 2004; Colombatti et al., 2000, 2011). Here, we show specifically that Mmrn1 expression is significantly reduced throughout placental development in *Egfl7*$^{-/-}$ mice. Mmrn1 has primarily been studied in humans for its role as a carrier protein for platelets (Jeimy et al., 2008; Tasneem et al., 2009); however, its precise role in the vasculature remains unknown. As Mmrn1 and Egfl7 are both associated with the ECM and share an EMI domain, it is possible that they interact and together exert an effect on the integrity of the ECM. Expression of other Emilin family genes was also significantly reduced in *Egfl7*$^{-/-}$ placentas at some, but not all, developmental stages examined (Mmrn2 and Emilin1 at E9.5; Emilin3 at E8.5). Intriguingly, Rossi and colleagues showed that the lack of vascular phenotypes in *egfl7* mutant zebrafish could be explained by compensatory upregulation of *emilin3a*, *emilin3b* and *emilin2a*, and that *emilin2* and *emilin3* could rescue the vascular defects observed in *egfl7* morphant embryos (Rossi et al., 2015). However, we did not observe upregulation of any of the known murine Emilin family genes in *Egfl7*$^{-/-}$ embryos, suggesting that potential compensatory mechanisms differ between mouse and zebrafish.

Our studies uncover, for the first time, a crucial functional role for Egfl7 in embryonic growth and in the developing placental vasculature in a loss-of-function mouse model that maintains miR-126 expression. These results provide novel insight into potential etiological factors underlying pathological placentation in humans, including IUGR and PE, which are leading causes of maternal and fetal morbidity and mortality. Uteroplacental vascular insufficiency, the main cause of IUGR, results in chronic oxygen and nutrient deprivation. Fetal circulatory adaptations compensate for growth restriction, but also program the fetus for increased risk of hypertension, cardiovascular disease and type 2 diabetes later in life (Osmond and Barker, 2000; Cohen et al., 2016). It would be of interest to determine whether the IUGR observed in *Egfl7*$^{-/-}$ embryos is linked to morbidities in the adult. Interestingly, elevated Egfl7 mRNA has been detected in maternal plasma of human pregnancies with early onset IUGR (Zanello et al., 2013). Given that EGFL7 is secreted, it will be important to determine whether the protein is detectable in the serum of pregnant women, and whether its expression is dysregulated in pregnancies with placental pathologies, including preeclampsia and intrauterine growth restriction.

MATERIALS AND METHODS

Mice

All animal protocols were approved and are in accordance with the Institutional Animal Care and Use Committee (IACUC) at Weill Cornell Medical College of Cornell University. C57BL/6J mice were obtained from Jackson Laboratories. *Egfl7*$^{-/-}$ mice were derived at the Mouse Genetics Core at Memorial Sloan Kettering Cancer Center from *Egfl7* knockout embryonic stem cells (F1 [C57BL/6×126S6/SvEv] hybrid) provided by Nicholas Gale at Regeneron Pharmaceuticals (VelociGene modified allele ID1501) through a Research Collaboration Agreement

Development (2017) 144, 2469-2479 doi:10.1242/dev.147025

between Weill Medical College of Cornell University. A 13 bp region from the first ATG to 1 bp after the second ATG (5′-ATG CAG ACC ATG T-3′), was excised. See supplementary Materials and Methods for further information.

Founder mice were backcrossed into the C57BL/6J background for 10 generations to obtain congenic mice. For timed pregnancies, 8-10 week old mice were used with the date of the vaginal plug designated as E0.5.

Sequencing

Genomic DNA was amplified using specific primer sets surrounding the 13 bp deletion site, and purified samples were sequenced by the Cornell University Biotechnology Resource Center. See supplementary Materials and Methods for primer sequences and further information.

Immunohistochemistry

Placentas were isolated, fixed in 4% paraformaldehyde and embedded in an OCT:30% sucrose mixture in PBS (2:1) or dehydrated and embedded in paraffin wax for Hematoxylin and Eosin staining. For detailed staining protocols and antibody information, see supplementary Materials and Methods.

Microangiography

Females were sacrificed at E12.5 by cervical dislocation; conceptuses were isolated in L15 medium (Invitrogen) and umbilical arteries exposed. Tomato-lectin (Vector Labs, #DL-1177) (40 µl) in PBS containing heparin was injected into the umbilical artery. Each conceptus was incubated for 10 min at 37°C in L15 medium to allow the embryonic heart to circulate the injected dye throughout the feto-placental circulation. Placentas and embryos were then further dissected and fixed overnight at 4°C in 4% paraformaldehyde. Only conceptuses in which tomato-lectin had completely circulated through the placenta and reached the embryo were kept for analysis. Placentas were incubated in 5% low melt agarose for 2 h at 42°C, and embedded in 5% low melt agarose through solidification at room temperature. Blocks were cut on a vibratome at 100 µm. Agarose was removed and sections were either mounted in Prolong Gold (Life Technologies) using slide wells (Electron Microscopy Sciences) or processed for immunostaining. See supplementary Materials and Methods for further information regarding retrospective immunostaining.

Real-time RT-PCR

E8.5 pre-placental tissues (chorion, ectoplacental cone and decidua) and placentas (E9.5, E12.5) were flash frozen in liquid nitrogen. RNA was isolated using Trizol (Invitrogen) and reverse transcribed using qScript cDNA Synthesis Kit (Quanta Biosciences). Gene expression was measured quantitatively using PerfeCTa SYBR Green SuperMix for iQ (Quanta Biosciences). Specific primer sets are listed in Table S1. For analysis of miR-126 expression, TaqMan MicroRNA Reverse Transcription Kit (Life Technologies, 4366596) and TaqMan Universal PCR Master Mix (Life Technologies, 4324018) were used. See supplementary Materials and Methods for further information on real time RT-PCR analyses.

EdU labeling

Proliferating cells were labeled using the Click-iT EdU Imaging Kit (Life Technologies, C10339) at E12.5 of gestation. See supplementary Materials and Methods for further information.

Placental and embryonic endothelial cell cultures

Placental and embryonic ECs were isolated and activated as previously described (Kobayashi et al., 2010; Poulos et al., 2015), from timed pregnancies of C57BL/6J control and *Egfl7*$^{-/-}$ matings at E10.5. Placentas and embryos were digested with Collagenase/Dispase (Roche) and ECs were immunopurified using CD31-captured magnetic beads (Life Technologies). Cultures were transduced with a myristoylated-Akt1 expressing lentivirus (Kobayashi et al., 2010), expanded and cultured on fibronectin (Sigma-Aldrich)-coated plates. Purity was assessed by immunostaining. See supplementary Materials and Methods for further information.

Endothelial cell functional *in vitro* assays

Isolated endothelial cells were subjected to functional *in vitro* assays. For details on the scratch wound assay, the sprouting assay, the proliferation assay and the cord formation assay, see supplementary Materials and Methods.

Quantitative analysis of placental tissues

Fetal blood space area and morphological quantification was performed using Image J software. See supplementary Materials and Methods for further information.

Statistics

Data are represented as mean±s.e.m. The data were analyzed using Student's *t*-test or one-way ANOVA with Tukey's multiple comparison test. Statistical significance was defined as $*P<0.05$, $**P<0.01$, $***P<0.001$, or $****P<0.0001$.

Acknowledgements

We are grateful to Dr Nicholas W. Gale at Regeneron Pharmaceuticals for the mouse ESC clone containing the *Egfl7* knockout allele. We thank members of the Stuhlmann Laboratory, including Abhijeet Sharma, Kathryn Bambino, Lissenya B. Argueta and Trevor Lee, as well as Drs Nicholas Gale, Jenna Schmahl, David Frendewey, Doris Herzlinger and Luisa Campagnolo for comments on the manuscript. We thank Drs Ian Tattersall and Jan Kitajewski for advice on the fibrin gel bead assay, and Drs Paula Cohen and Miguel Brieno Enriquez for advice on sex determination. Technical support was provided by the MSK Mouse Genetics Core Facility, Cornell University Biotechnology Resources Center and WCMC Optical Microscopy Core facility.

Competing interests

The authors declare no competing or financial interests.

Author contributions

Conceptualization: L.A.L., H.S.; Methodology: L.A.L., R.H., S.H., M.G.P., J.M.B., H.S.; Software: L.A.L.; Validation: L.A.L., H.S.; Formal analysis: L.A.L., H.S.; Investigation: L.A.L., R.H., S.H., M.G.P., J.M.B., H.S.; Resources: R.H., H.S.; Data curation: L.A.L., R.H., H.S.; Writing - original draft: L.A.L., H.S.; Writing - review & editing: L.A.L., R.H., M.G.P., J.M.B., H.S.; Visualization: L.A.L.; Supervision: H.S.; Project administration: H.S.; Funding acquisition: R.H., H.S.

Funding

This work was supported by the National Institutes of Health (T32 HD060600 to L.A.L., R01 HL082098 to H.S., and P20-103072 and R01-DK45218 to R.H.) and by the March of Dimes Foundation (6-FY14-411 to H.S.) Deposited in PMC for release after 12 months.

Supplementary information

Supplementary information available online at
http://dev.biologists.org/lookup/doi/10.1242/dev.147025.supplemental

References

Anson-Cartwright, L., Dawson, K., Holmyard, D., Fisher, S. J., Lazzarini, R. A. and Cross, J. C. (2000). The glial cells missing-1 protein is essential for branching morphogenesis in the chorioallantoic placenta. *Nat. Genet.* **25**, 311-314.

Arnaoutova, I. and Kleinman, H. K. (2010). In vitro angiogenesis: endothelial cell tube formation on gelled basement membrane extract. *Nat. Protoc.* **5**, 628-635.

Bambino, K., Lacko, L. A., Hajjar, K. A. and Stuhlmann, H. (2014). Epidermal growth factor-like Domain 7 is a marker of the endothelial lineage and active angiogenesis. *Genesis* **52**, 657-670.

Braghetta, P., Ferrari, A., De Gemmis, P., Zanetti, M., Volpin, D., Bonaldo, P. and Bressan, G. M. (2004). Overlapping, complementary and site-specific expression pattern of genes of the emilin/multimerin family. *Matrix Biol.* **22**, 549-556.

Campagnolo, L., Leahy, A., Chitnis, S., Koschnick, S., Fitch, M. J., Fallon, J. T., Loskutoff, D., Taubman, M. B. and Stuhlmann, H. (2005). Egfl7 is a chemoattractant for endothelial cells and is up-regulated in angiogenesis and arterial injury. *Am. J. Pathol.* **167**, 275-284.

Campagnolo, L., Moscatelli, I., Pellegrini, M., Siracusa, G. and Stuhlmann, H. (2008). Expression of egfl7 in primordial germ cells and in adult ovaries and testes. *Gene Expr. Patterns* **8**, 389-396.

Cohen, E., Wong, F. Y., Horne, R. S. C. and Yiallourou, S. R. (2016). Intrauterine growth restriction: impact on cardiovascular development and function throughout infancy. *Pediatr. Res.* **79**, 821-830.

Colombatti, A., Doliana, R., Bot, S., Canton, A., Mongiat, M., Mungiguerra, G., Paron-Cilli, S. and Spessotto, P. (2000). The emilin protein family. *Matrix Biol.* **19**, 289-301.

Colombatti, A., Spessotto, P., Doliana, R., Mongiat, M., Bressan, G. M. and Esposito, G. (2011). The Emilin/Multimerin family. *Front Immunol* **2**, 93.
Cross, J. C., Nakano, H., Natale, D. R. C., Simmons, D. G. and Watson, E. D. (2006). Branching morphogenesis during development of placental villi. *Differentiation* **74**, 393-401.
Downs, K. M. and Gardner, R. L. (1995). An investigation into early placental ontogeny: allantoic attachment to the chorion is selective and developmentally regulated. *Development* **121**, 407-416.
Dupressoir, A., Marceau, G., Vernochet, C., Bénit, L., Kanellopoulos, C., Sapin, V. and Heidmann, T. (2005). Syncytin-a and syncytin-b, two fusogenic placenta-specific murine envelope genes of retroviral origin conserved in muridae. *Proc. Natl. Acad. Sci. USA* **102**, 725-730.
Dupressoir, A., Vernochet, C., Bawa, O., Harper, F., Pierron, G., Opolon, P. and Heidmann, T. (2009). Syncytin-a knockout mice demonstrate the critical role in placentation of a fusogenic, endogenous retrovirus-derived, envelope gene. *Proc. Natl. Acad. Sci. USA* **106**, 12127-12132.
Dupressoir, A., Vernochet, C., Harper, F., Guégan, J., Dessen, P., Pierron, G. and Heidmann, T. (2011). A pair of co-opted retroviral envelope syncytin genes is required for formation of the two-layered murine placental syncytiotrophoblast. *Proc. Natl. Acad. Sci. USA* **108**, E1164-E1173.
Fish, J. E., Santoro, M. M., Morton, S. U., Yu, S., Yeh, R.-F., Wythe, J. D., Ivey, K. N., Bruneau, B. G., Stainier, D. Y. R. and Srivastava, D. (2008). Mir-126 regulates angiogenic signaling and vascular integrity. *Dev. Cell* **15**, 272-284.
Fitch, M. J., Campagnolo, L., Kuhnert, F. and Stuhlmann, H. (2004). Egfl7, a novel epidermal growth factor-domain gene expressed in endothelial cells. *Dev. Dyn.* **230**, 316-324.
Jeimy, S. B., Fuller, N., Tasneem, S., Segers, K., Stafford, A. R., Weitz, J. I., Camire, R. M., Nicolaes, G. A. and Hayward, C. P. (2008). Multimerin 1 binds factor V and activated factor V with high affinity and inhibits thrombin generation. *Thromb. Haemost.* **100**, 1058-1067.
Junus, K., Centlow, M., Wikström, A.-K., Larsson, I., Hansson, S. R. and Olovsson, M. (2012). Gene expression profiling of placentae from women with early- and late-onset pre-eclampsia: down-regulation of the angiogenesis-related genes ACVRL1 and EGFL7 in early-onset disease. *Mol. Hum. Reprod.* **18**, 146-155.
Kobayashi, H., Butler, J. M., O'donnell, R., Kobayashi, M., Ding, B.-S., Bonner, B., Chiu, V. K., Nolan, D. J., Shido, K., Benjamin, L. et al. (2010). Angiocrine factors from akt-activated endothelial cells balance self-renewal and differentiation of haematopoietic stem cells. *Nat. Cell Biol.* **12**, 1046-1056.
Kubota, Y., Kleinman, H. K., Martin, G. R. and Lawley, T. J. (1988). Role of laminin and basement membrane in the morphological differentiation of human endothelial cells into capillary-like structures. *J. Cell Biol.* **107**, 1589-1598.
Kuhnert, F., Mancuso, M. R., Hampton, J., Stankunas, K., Asano, T, Chen, C.-Z. and Kuo, C. J. (2008). Attribution of vascular phenotypes of the murine Egfl7 locus to the microrna mir-126. *Development* **135**, 3989-3993.
Lacko, L. A., Massimiani, M., Sones, J. L., Hurtado, R., Salvi, S., Ferrazzani, S., Davisson, R. L., Campagnolo, L. and Stuhlmann, H. (2014). Novel expression of Egfl7 in placental trophoblast and endothelial cells and its implication in preeclampsia. *Mech. Dev.* **133**, 163-176.
Lelièvre, E., Hinek, A., Lupu, F., Buquet, C., Soncin, F. and Mattot, V. (2008). Ve-statin/Egfl7 regulates vascular elastogenesis by interacting with lysyl oxidases. *EMBO J.* **27**, 1658-1670.
Liang, C.-C., Park, A. Y. and Guan, J.-L. (2007). In vitro scratch assay: a convenient and inexpensive method for analysis of cell migration in vitro. *Nat. Protoc.* **2**, 329-333.
Massimiani, M., Vecchione, L., Piccirilli, D., Spitalieri, P., Amati, F., Salvi, S., Ferrazzani, S., Stuhlmann, H. and Campagnolo, L. (2015). Epidermal growth factor-like domain 7 promotes migration and invasion of human trophoblast cells through activation of mapk, Pi3k and notch signaling pathways. *Mol. Hum. Reprod.* **21**, 435-451.
Nakatsu, M. N. and Hughes, C. C. W. (2008). An optimized three-dimensional in vitro model for the analysis of angiogenesis. *Methods Enzymol.* **443**, 65-82.
Nehls, V. and Drenckhahn, D. (1995). A novel, microcarrier-based in vitro assay for rapid and reliable quantification of three-dimensional cell migration and angiogenesis. *Microvasc. Res.* **50**, 311-322.
Nichol, D. and Stuhlmann, H. (2012). Egfl7: a unique angiogenic signaling factor in vascular development and disease. *Blood* **119**, 1345-1352.
Nichol, D., Shawber, C., Fitch, M. J., Bambino, K., Sharma, A., Kitajewski, J. and Stuhlmann, H. (2010). Impaired angiogenesis and altered notch signaling in mice overexpressing endothelial Egfl7. *Blood* **116**, 6133-6143.
Nolan, D. J., Ginsberg, M., Israely, E., Palikuqi, B., Poulos, M. G., James, D., Ding, B.-S., Schachterle, W., Liu, Y., Rosenwaks, Z. et al. (2013). Molecular signatures of tissue-specific microvascular endothelial cell heterogeneity in organ maintenance and regeneration. *Dev. Cell* **26**, 204-219.
Osmond, C. and Barker, D. J. (2000). Fetal, infant, and childhood growth are predictors of coronary heart disease, diabetes, and hypertension in adult men and women. *Environ. Health Perspect* **108** Suppl 3, 545-553.
Parker, L. H., Schmidt, M., Jin, S.-W., Gray, A. M., Beis, D., Pham, T., Frantz, G., Palmieri, S., Hillan, K., Stainier, D. Y. R. et al. (2004). The endothelial-cell-derived secreted factor Egfl7 regulates vascular tube formation. *Nature* **428**, 754-758.
Poulos, M. G., Crowley, M. J. P., Gutkin, M. C., Ramalingam, P., Schachterle, W., Thomas, J.-L., Elemento, O. and Butler, J. M. (2015). Vascular platform to define hematopoietic stem cell factors and enhance regenerative hematopoiesis. *Stem Cell Reports* **5**, 881-894.
Rossant, J. and Cross, J. C. (2001). Placental development: lessons from mouse mutants. *Nat. Rev. Genet.* **2**, 538-548.
Rossi, A., Kontarakis, Z., Gerri, C., Nolte, H., Hölper, S., Krüger, M. and Stainier, D. Y. (2015). Genetic compensation induced by deleterious mutations but not gene knockdowns. *Nature* **524**, 230-233.
Sakai, K. and Miyazaki, J.-i. (1997). A transgenic mouse line that retains cre recombinase activity in mature oocytes irrespective of the Cre transgene transmission. *Biochem. Biophys. Res. Commun.* **237**, 318-324.
Schmidt, M. H. H., Bicker, F., Nikolic, I., Meister, J., Babuke, T., Picuric, S., Müller-Esterl, W., Plate, K. H. and Dikic, I. (2009). Epidermal growth factor-like domain 7 (Egfl7) modulates notch signalling and affects neural stem cell renewal. *Nat. Cell Biol.* **11**, 873-880.
Sharma, D., Shastri, S., Farahbakhsh, N. and Sharma, P. (2016a). Intrauterine growth restriction - Part 1. *J. Matern. Fetal. Neonatal. Med.* **29**, 3977-3987.
Sharma, D., Shastri, S. and Sharma, P. (2016b). Intrauterine growth restriction: antenatal and postnatal aspects. *Clin. Med. Insights Pediatr.* **10**, 67-83.
Soncin, F., Mattot, V., Lionneton, F., Spruyt, N., Lepretre, F., Begue, A. and Stehelin, D. (2003). Ve-statin, an endothelial repressor of smooth muscle cell migration. *EMBO J.* **22**, 5700-5711.
Tasneem, S., Adam, F., Minullina, I., Pawlikowska, M., Hui, S. K., Zheng, S., Miller, J. L. and Hayward, C. P. (2009). Platelet adhesion to multimerin 1 in vitro: influences of platelet membrane receptors, von Willebrand factor and shear. *J. Thromb. Haemost.* **7**, 685-692.
Tattersall, I. W., Du, J., Cong, Z., Cho, B. S., Klein, A. M., Dieck, C. L., Chaudhri, R. A., Cuervo, H., Herts, J. H. and Kitajewski, J. (2016). In vitro modeling of endothelial interaction with macrophages and pericytes demonstrates notch signaling function in the vascular microenvironment. *Angiogenesis* **19**, 201-215.
Valenzuela, D. M., Murphy, A. J., Frendewey, D., Gale, N. W., Economides, A. N., Auerbach, W., Poueymirou, W. T., Adams, N. C., Rojas, J., Yasenchak, J. et al. (2003). High-throughput engineering of the mouse genome coupled with high-resolution expression analysis. *Nat. Biotechnol.* **21**, 652-659.
Wang, S., Aurora, A. B., Johnson, B. A., Qi, X., Mcanally, J., Hill, J. A., Richardson, J. A., Bassel-Duby, R. and Olson, E. N. (2008). The endothelial-specific microrna Mir-126 governs vascular integrity and angiogenesis. *Dev. Cell* **15**, 261-271.
Watson, E. D. and Cross, J. C. (2005). Development of structures and transport functions in the mouse placenta. *Physiology (Bethesda)* **20**, 180-193.
Young, B. C., Levine, R. J. and Karumanchi, S. A. (2010). Pathogenesis of preeclampsia. *Annu. Rev. Pathol.* **5**, 173-192.
Zanello, M., Desanctis, P., Pula, G., Zucchini, C., Pittalis, M. C., Rizzo, N. and Farina, A. (2013). Circulating Mrna for epidermal growth factor-like domain 7 (Egfl7) in maternal blood and early intrauterine growth restriction. a preliminary analysis. *Prenat. Diagn.* **33**, 168-172.

Supplemental Figures

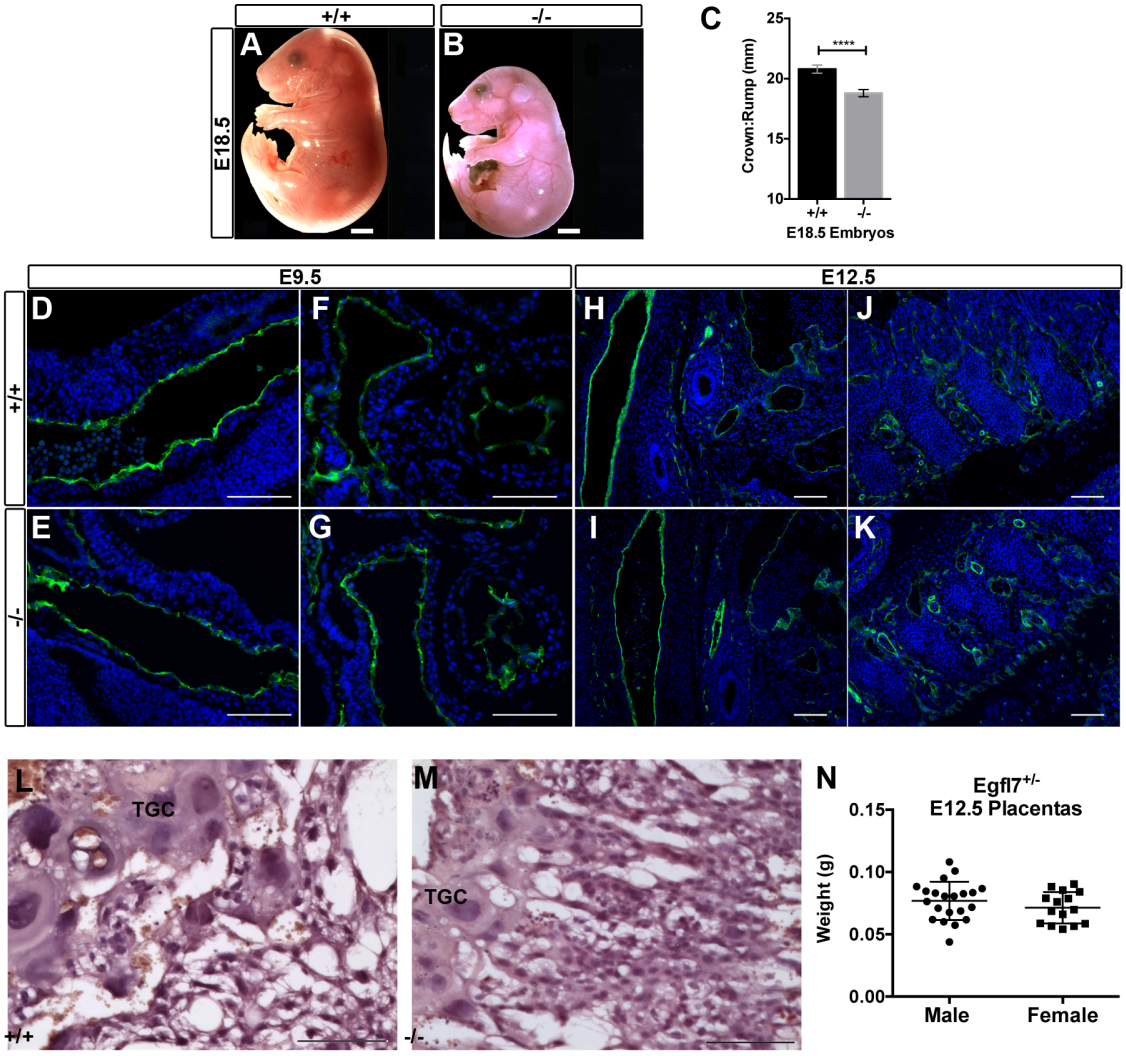

FIG. S1. Morphological analyses of *Egfl7*$^{-/-}$ embryos and placentas. (A-B) Representative images of E18.5 C57BL/6J and *Egfl7*$^{-/-}$ embryos. (C) Quantification of the crown-to-rump length of E18.5 C57BL/6J (n=29) and *Egfl7*$^{-/-}$ (n=23) embryos showing fetal growth restriction. (D-K) Immunofluorescent staining for CD31 (green) and DAPI (blue) on sections of E9.5 (D-G) and E12.5 (H-K) C57BL/6J (+/+, D,F,H,J) and *Egfl7*$^{-/-}$ (E,G,I,K) embryos, depicting a lack of gross vascular defects. High magnification images of the developing aorta (D-E, H-I), heart (F-G), and intersomitic vessels (J-K). (L-M) High magnification images of the junctional zone of hematoxylin and eosin stained paraffin sections of E12.5 C57BL/6J control (+/+) and *Egfl7*$^{-/-}$ placentas. TGC-trophoblast giant cell. (N) Analysis of Egfl7+/- male and female placental weights at E12.5

suggesting no difference in sexual dimporphic imprinting. Data were analyzed using student's t-test and represented as mean ± SEM. ****P<0.0001 Scale bars= 100μm.

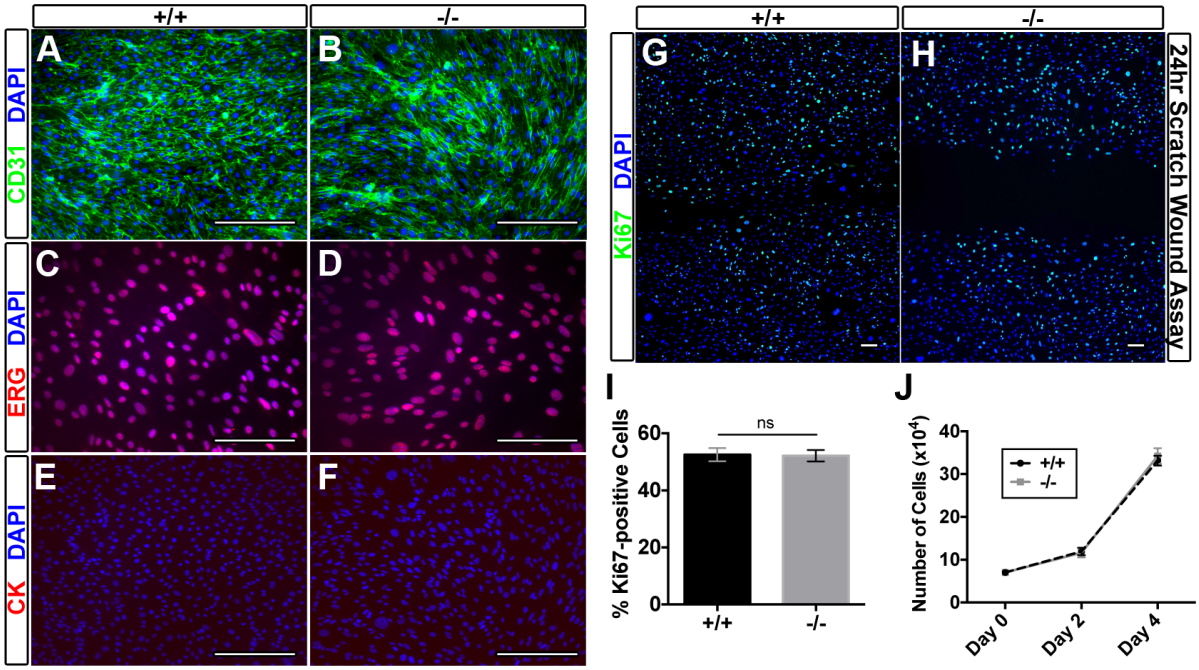

FIG. S2. Characterization of isolated placental endothelial cells. Representative images of C57BL/6J (+/+) (A,C,E) and *Egfl7*$^{-/-}$ (B,D,F) isolated placental endothelial cells stained for endothelial markers, CD31 (green, A-B) and ERG (red, C-D), trophoblast marker, CYTOKERATIN (red, E-F), and nuclear DAPI (blue) (n=3 from three independent experiments). Immunostaining demonstrates the cell cultures are >99% pure. (G-H) Representative images of C57BL/6J (+/+) (G) and *Egfl7*$^{-/-}$ (H) placental endothelial cells stained for proliferation marker, Ki67 (green), and DAPI (blue) during the scratch wound assay. (I) Quantification of the percentage of Ki67-positive cells in the scratch wound assay showing no significant difference between C57BL/6J controls and *Egfl7*$^{-/-}$ placental endothelial cells (+/+ n=6; -/- n=6). (J) Proliferation rates of isolated placental endothelial cell cultures from C57BL/6J control and *Egfl7*$^{-/-}$ placentas (+/+ n=9; -/- n=9). Data were analyzed using student's t-test and represented as mean ± SEM. Scale bars= 100μm.

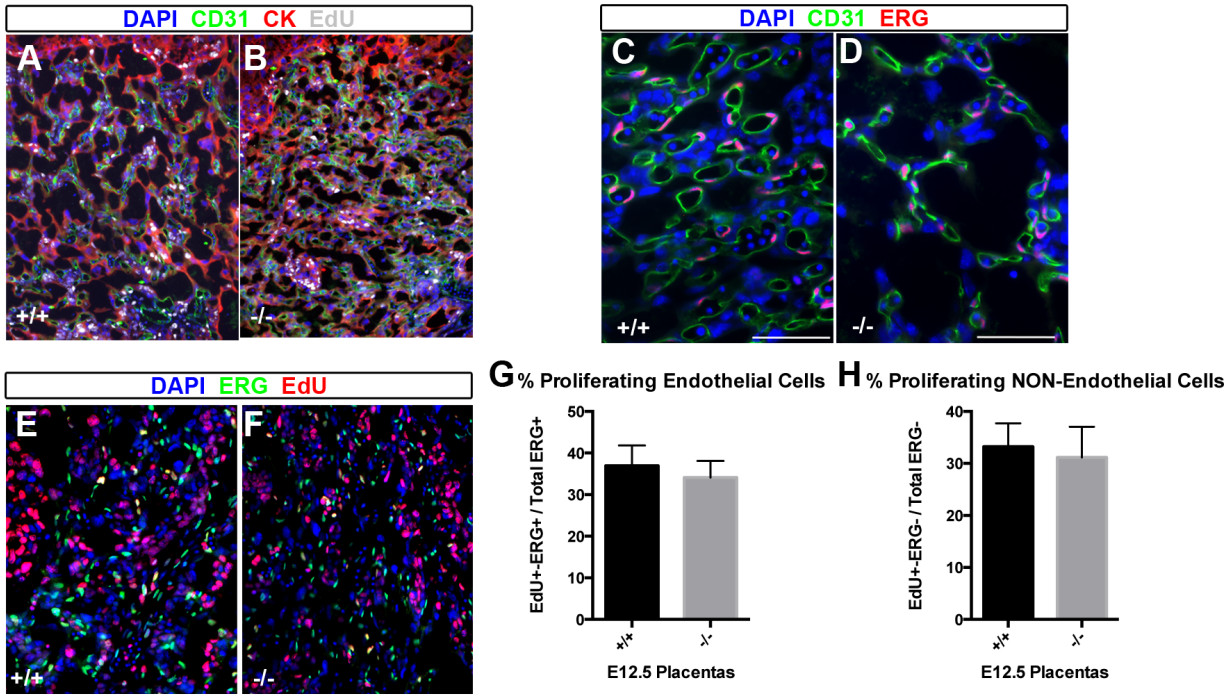

FIG. S3. Proliferation of placental endothelial and trophoblast cells is not affected by Egfl7 loss-of-function *in vivo*. Representative merged images of the E12.5 fetal labyrinth of (A) C57BL/6J (+/+) and (B) *Egfl7*$^{-/-}$ placentas immunostained for EdU (white), CD31 (green), CYTOKERATIN (red) and nuclear DAPI (blue). (C-D) Representative merged images of the E12.5 fetal labyrinth of C57BL/6J (+/+) and *Egfl7*$^{-/-}$ placentas immunostained for ERG (red), CD31 (green) and nuclear DAPI (blue), demonstrating that all ERG-positive cells in the fetal labyrinth are also CD31-positive. (E-F) Representative merged images of the E12.5 fetal labyrinth of C57BL/6J (+/+) and *Egfl7*$^{-/-}$ placentas immunostained for EdU (red), endothelial ERG (green) and nuclear DAPI (blue). (G-H) Quantification of proliferating endothelial and non-endothelial cells in the fetal labyrinth of E12.5 placentas (+/+, n=3; -/-, n=3). No significant difference in proliferating endothelial (G) and non-endothelial cells (H) was observed. Data were analyzed using student's t-test and represented as mean ± SEM.

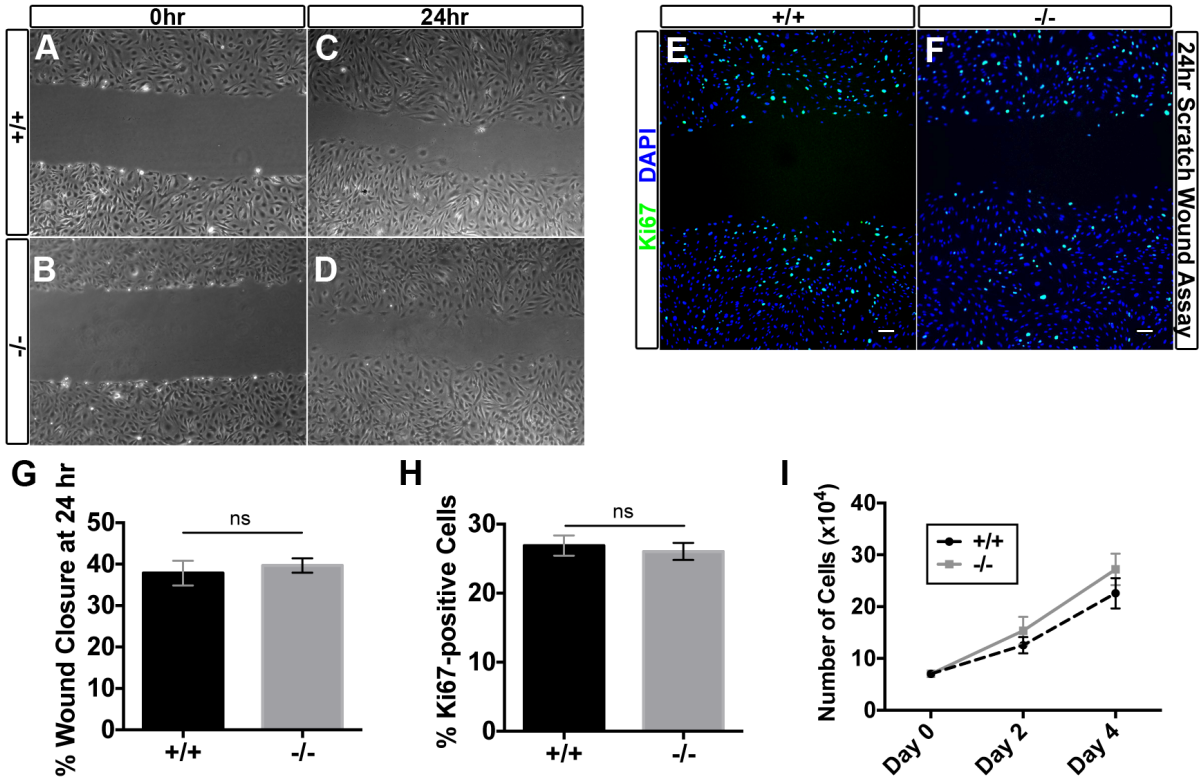

FIG. S4. Characterization of *Egfl7*$^{-/-}$ embryonic endothelial cells. Isolated E10.5 embryonic endothelial cells (ECs) from C57BL/6J control (+/+) and *Egfl7*$^{-/-}$ mice were used for functional EC assays *in vitro*. (A-D) Representative images of embryonic ECs grown to confluency and subjected to a scratch-wound healing assay. Collective EC migration was observed at 24hr (C-D). (E-F) Representative images of C57BL/6J (+/+) control (E) and *Egfl7*$^{-/-}$ (F) embryonic endothelial cells stained for proliferation marker, Ki67 (green), and DAPI (blue) during the scratch wound assay. (G) Quantification of the percentage of wound area closed by migrating ECs at 24hr (+/+, n=18; -/-, n=18). (H) Quantification of the percentage of Ki67-positive cells in the scratch wound assay showing no significant difference between C57BL/6J controls and *Egfl7*$^{-/-}$ embryonic endothelial cells (+/+ n=6; -/- n=6). (I) Proliferation rates of isolated embryonic endothelial cell cultures from C57BL/6J control and *Egfl7*$^{-/-}$ placentas (+/+ n=6; -/- n=6). Data were analyzed using student's t-test and represented as mean ± SEM. Scale bars= 100μm.

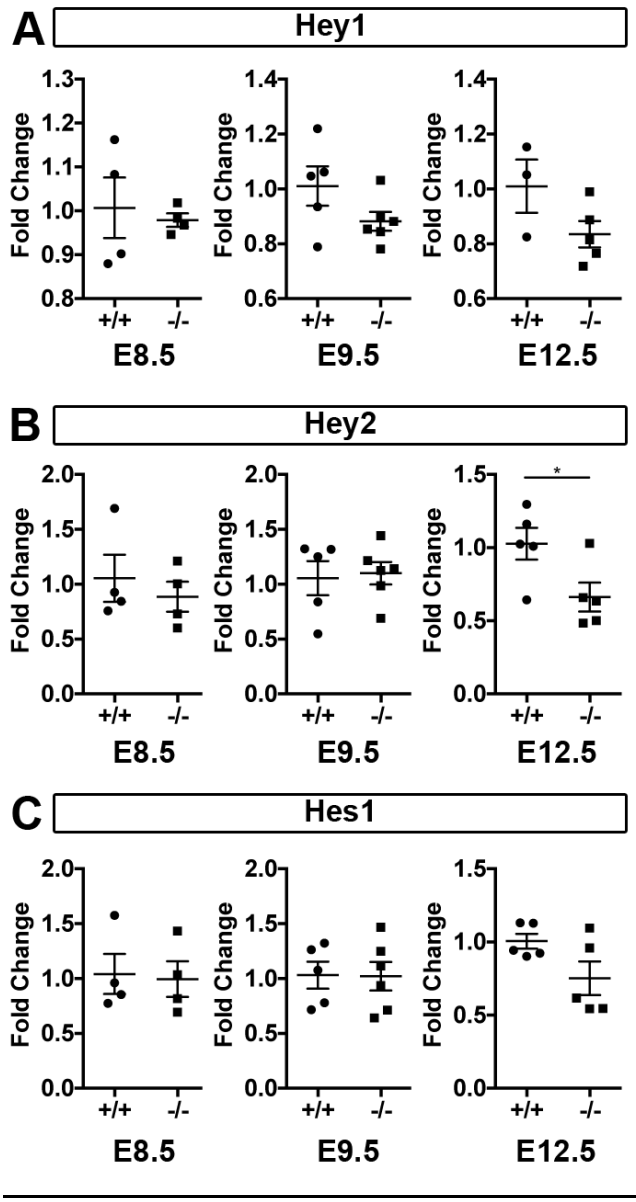

FIG. S5. Notch signaling in the developing placenta of C57BL/6J and *Egfl7*$^{-/-}$ mice. Real Time RT-PCR for Hey1 (A), Hey2 (B), and Hes1 (C) on pre-placental tissues and placentas from C57BL/6J (+/+) and *Egfl7*$^{-/-}$ mice at E8.5, E9.5, and E12.5 (n=4-5). Data were analyzed using student's t-test and represented as mean ± SEM. *P<0.05

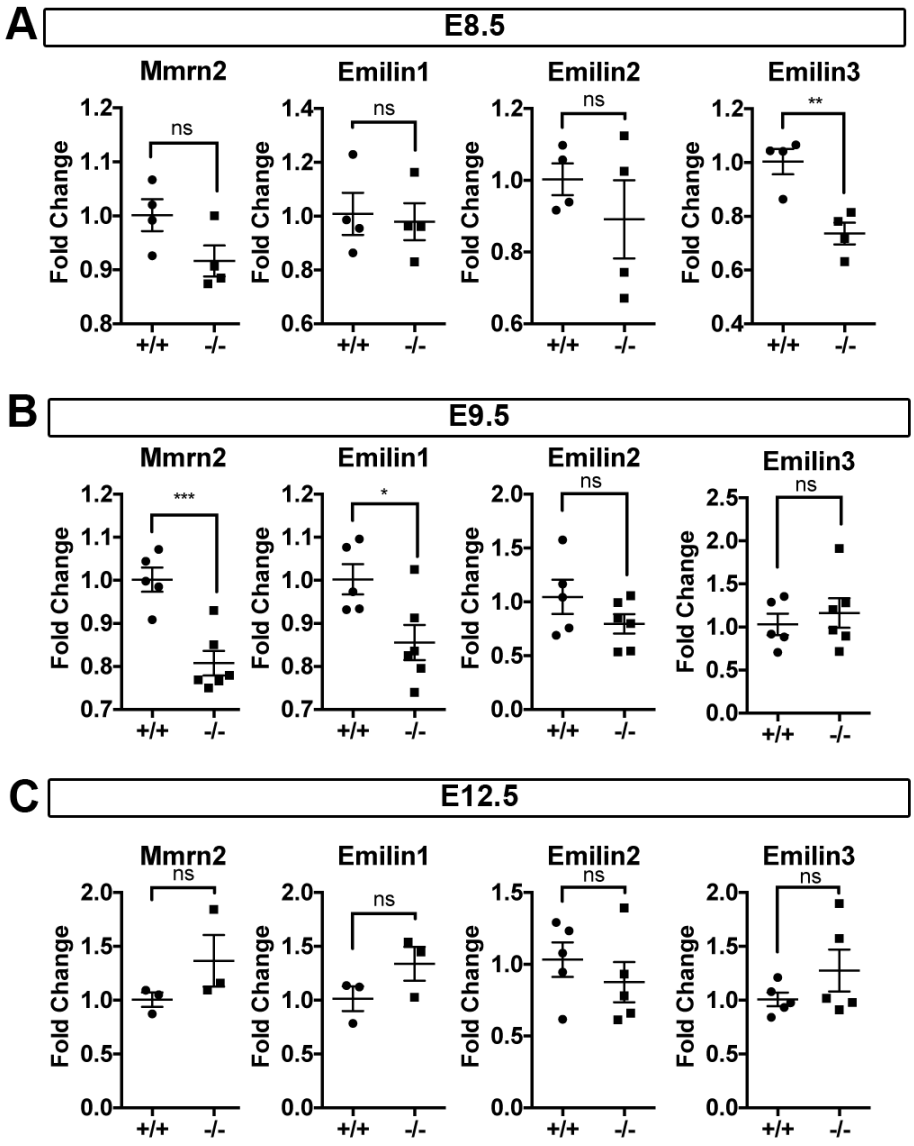

FIG. S6. Emilin family gene transcript levels in E8.5, E9.5 and E12.5 C57BL/6J and *Egfl7*$^{-/-}$ pre-placental tissues and placentas. Real Time RT-PCR for Emilin family genes Mmrn2, Emilin1, Emilin2, and Emilin3, on pre-placental tissues and placentas from C57BL/6J (+/+) and *Egfl7*$^{-/-}$ mice at E8.5 (A), E9.5 (B) and E12.5 (B) (n=3-6). Data were analyzed using student's t-test and represented as mean ± SEM. **P*<0.05, ***P*<0.01, ****P*<0.001

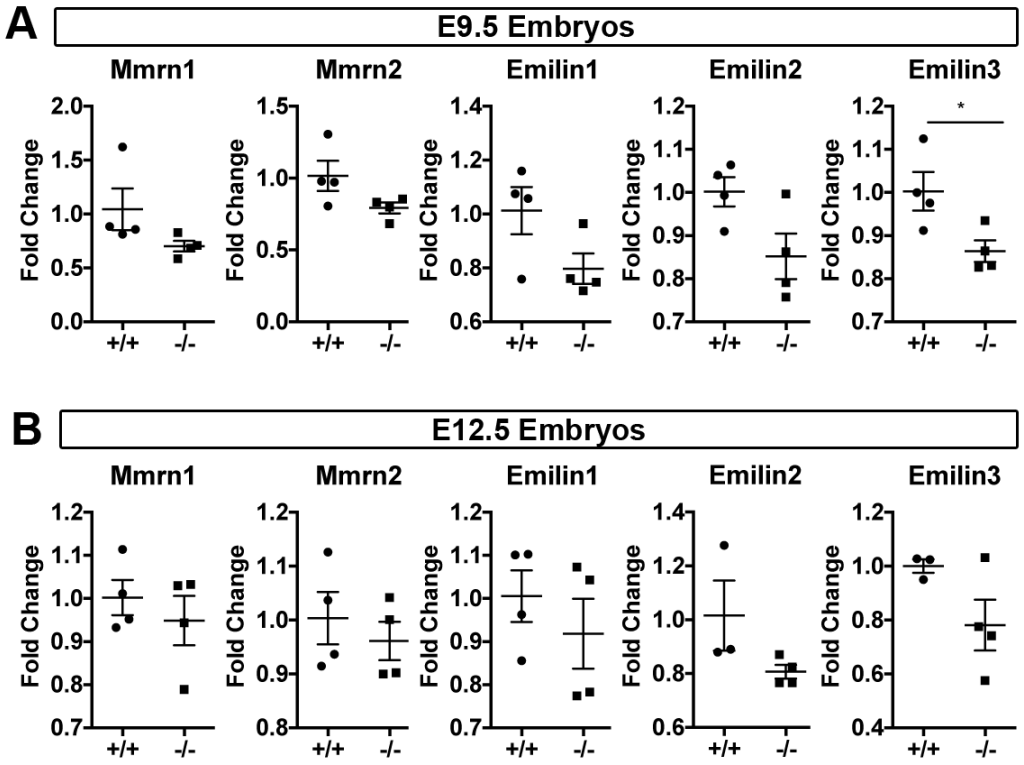

FIG. S7. Emilin family gene transcript levels in E9.5 and E12.5 C57BL/6J and *Egfl7*$^{-/-}$ embryos. Real Time RT-PCR for Emilin family genes Mmrn1, Mmrn2, Emilin1, Emilin2, and Emilin3, on embryos from C57BL/6J (+/+) and *Egfl7*$^{-/-}$ mice at E9.5 (A) and E12.5 (B) (n=4). Data were analyzed using student's t-test and represented as mean ± SEM. *P<0.05

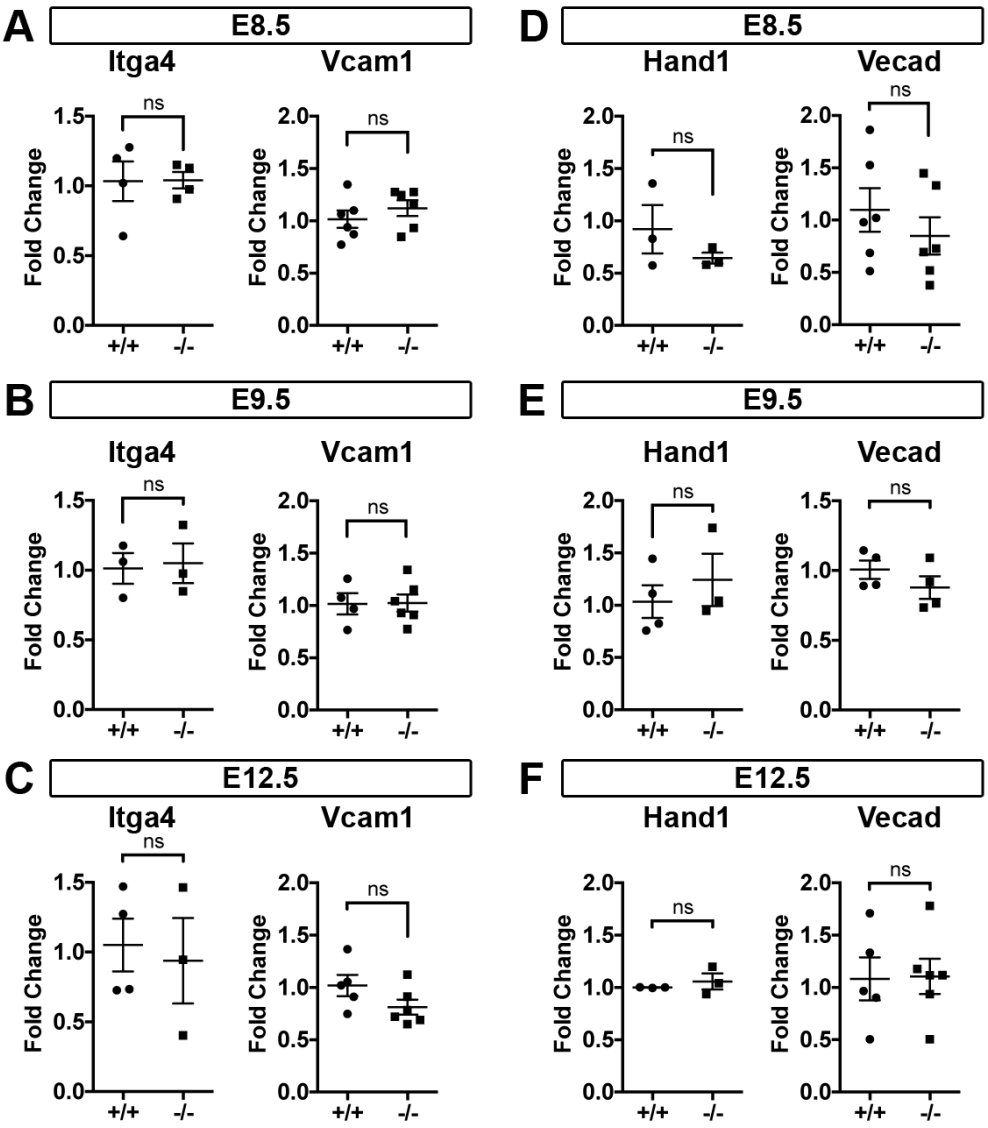

FIG. S8. Gene transcript levels in E8.5, E9.5 and E12.5 C57BL/6J and *Egfl7*$^{-/-}$ pre-placental tissues and placentas. Real Time RT-PCR on pre-placental tissues and placentas from C57BL/6J (+/+) and *Egfl7*$^{-/-}$ mice at E8.5 (A,D), E9.5 (B,E) and E12.5 (C,F), for branching morphogenesis genes Itga4 and Vcam1 (A-C), and genes with unrelated roles in placental development, including Hand1 and Vecad (D-F). Data were analyzed using student's t-test and represented as mean ± SEM.

Table S1

	Forward Primer (5'->3')	Reverse Primer (5'->3')	Reference if previously published
Egfl7	AGAGGAGGTGTACAGGCTGCA	TTCGGTCCAGCTGCTGGAAGGAAT	Nichol et al 2010
Egfl7 Δ13bp	ATGCAGACCATGTGGGGCTC	GGTCTCCGAGATGGAACCTCCG	N/A
Gcm1	CCCCAGCAAGTTCCATCAGA	AAGGCTCACCTCCCGGATT	Lu et al 2013
SynB	CCACCACCCATACGTTCAAA	GGTTATAGCAGGTGCCGAAG	Lu et al 2013
SynA	CCCTCATGGCTCCCATTCTC	TCATTCGCCGCGATACAGAA	N/A
Mmrn1	TGCAAGGGAAACACACCTCA	AGCACACCAATTCTTCCCTCT	N/A
Mmrn2	GAGTCATGTATCGAGTGGCCC	GATTGTGGTCCTGGCAGTCT	N/A
Emilin1	TGCCTACGTGGTGACTCGG	TCCGGTACATGATACTTCGGGA	N/A
Emilin2	CAGTGCCAGGAACAAAAACTGG	AACTCTCGCTTCCCTCCTGTA	N/A
Emilin3	CCTCAGATTCCCTTGGGGCAG	ATGACCCCAAAGCCACGGG	N/A (Note: only variant 2)
Hes1	AAAGCCTATCATGGAGAAGAGGCG	GGAATGCCGGGAGCTATCTTTCTTT	Nichol et al 2010
Hey1	TGAGCTGAGAAGGCTGGTAC	ACCCCAAACTCCGATAGTCC	Nichol et al 2010
Hey2	TGGGCATCAAAGTAGCCTTTA	TGAGAAGACTAGTGCCAACAGC	Nichol et al 2010
Itga4	AATCTCCTCCACCTACTCACAGAG	ACCAACGGCTACATCAACATATCC	Lu et al 2013
Vcam1	CGACCTTCATCCCCACCATT	GGGGGCAACGTTGACATAAAG	N/A
Hand1	AAAAGGGAGTTGCCTCAGCAG	GTTTAGCTCCAGCGCCCA	N/A
Vecad	ACTGGAACCAGCACGCTAAC	CAACTGCTCGTGAATCTCCA	Bambino et al 2014

Supplemental Movies

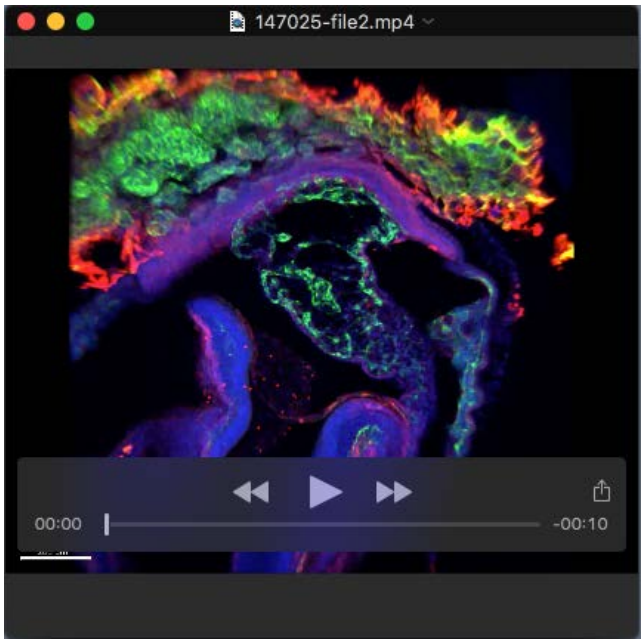

Movie S1. Chorionioallantoic branching morphogenesis of E8.5 C57BL/6J control conceptuses. Three-dimensional reconstruction of z-stack confocal images of 100μm thick vibratome sections of E8.5 C57BL/6J control conceptuses immunostained for CD31 (green), CYTOKERATIN (red) and nuclear DAPI (blue). Scale bar = 200μm.

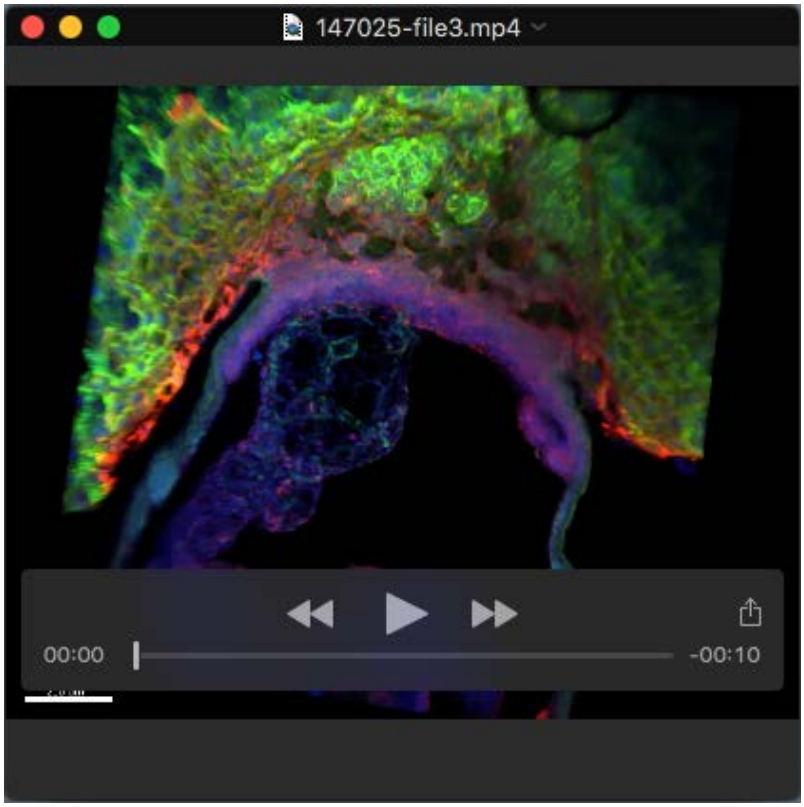

Movie S2. Chorionioallantoic branching morphogenesis of E8.5 *Egfl7*$^{-/-}$ conceptuses.
Three-dimensional reconstruction of z-stack confocal images of 100μm thick vibratome sections of E8.5 *Egfl7*$^{-/-}$ conceptuses immunostained for CD31 (green), CYTOKERATIN (red) and nuclear DAPI (blue), showing reduced percentage of chorioallantoic attachment. Scale bar = 200μm.

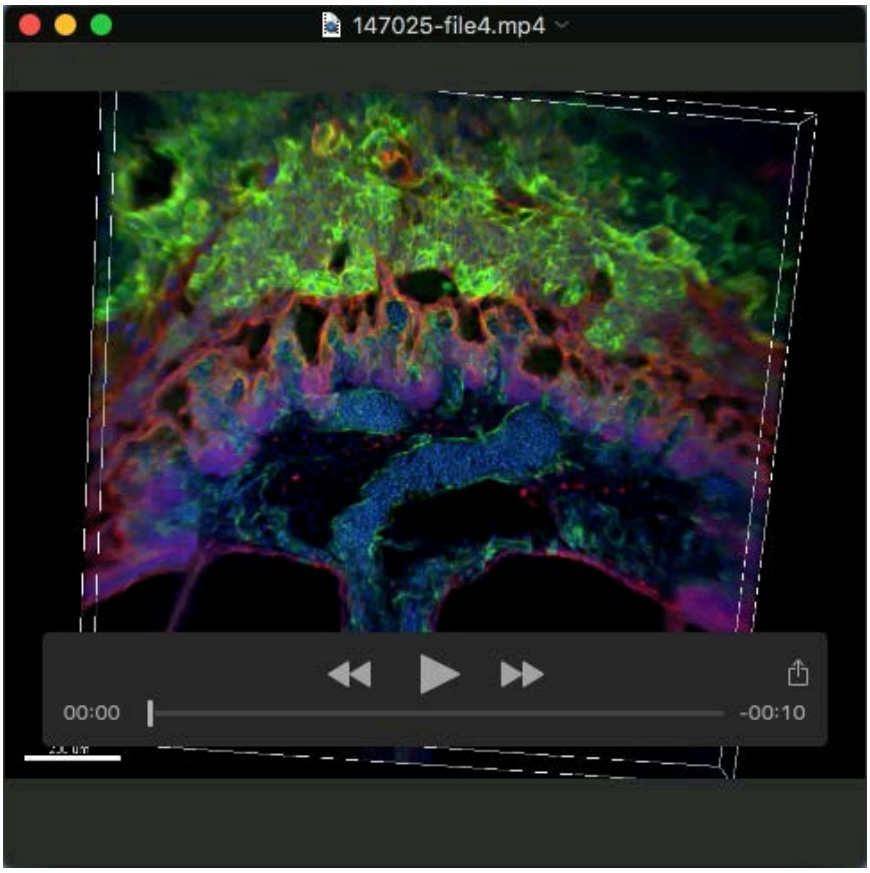

Movie S3. Chorionic invaginations of E9.5 C57BL/6J control placentas. Three-dimensional reconstruction of z-stack confocal images of 100μm thick vibratome sections of E9.5 C57BL/6J control conceptuses immunostained for CD31 (green), CYTOKERATIN (red) and nuclear DAPI (blue). Scale bar = 200μm.

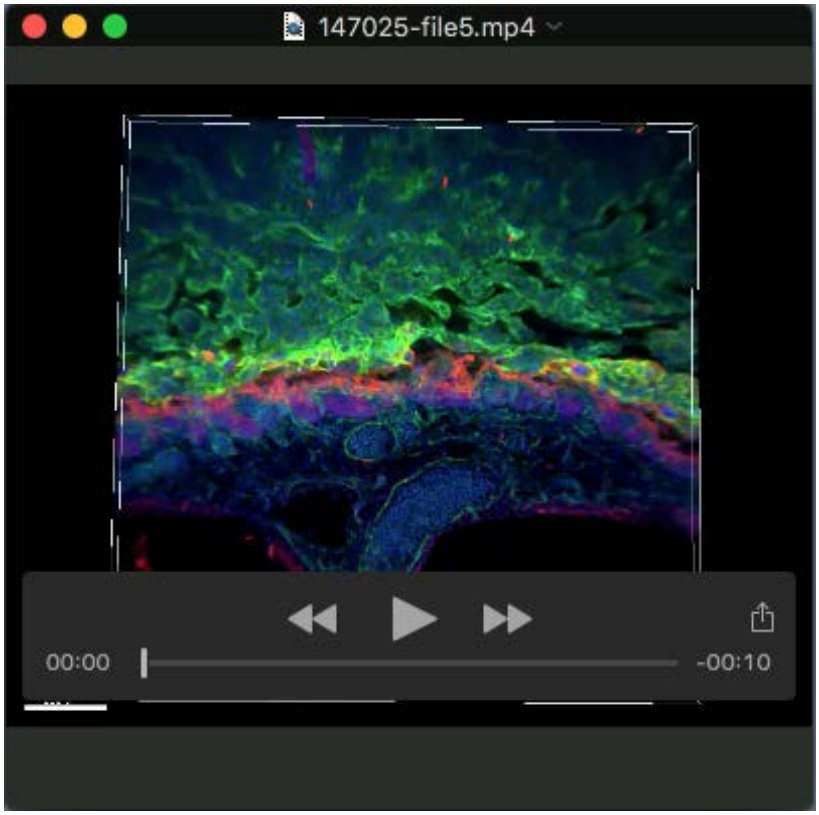

Movie S4. Chorionic invaginations of E9.5 *Egfl7*$^{-/-}$ placentas. Three-dimensional reconstruction of z-stack confocal images of 100μm thick vibratome sections of E9.5 *Egfl7*$^{-/-}$ conceptuses immunostained for CD31 (green), CYTOKERATIN (red) and nuclear DAPI (blue), showing reduced number of chorionic invaginations. Scale bar = 200μm.

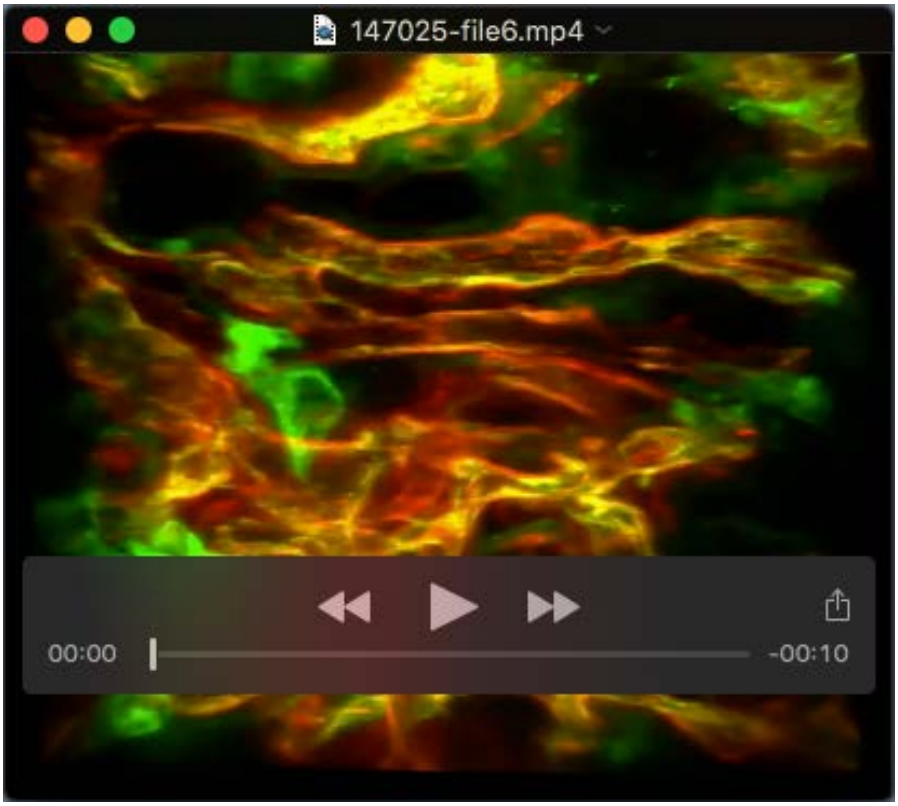

Movie S5. Microangiography of E12.5 C57BL/6J control placentas. Three-dimensional reconstruction of z-stack confocal images of E12.5 C57BL/6J control placentas perfused with tomato-lectin (red) and subsequently immunostained with CD31 (green).

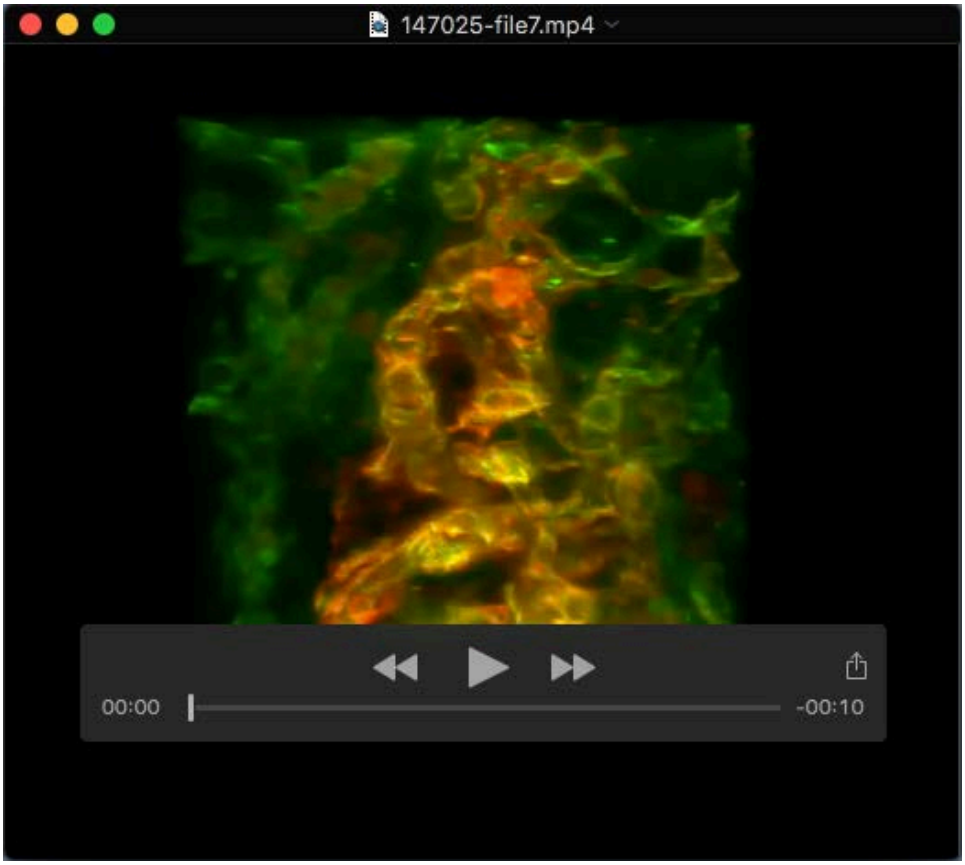

Movie S6. Microangiography of E12.5 *Egfl7*$^{-/-}$ placentas. Three-dimensional reconstruction of z-stack confocal images of E12.5 *Egfl7*$^{-/-}$ placentas perfused with tomato-lectin (red) and subsequently immunostained with CD31 (green) showing areas of feto- malperfusion.

Supplemental Materials and Methods

Mice

Egfl7$^{-/-}$ mice were derived as follows. VelociGene modified allele ID 1501 was produced with VelociGene methods (Valenzuela et al., 2003). A 13-bp region from the first ATG to 1 bp after the second ATG (5'-ATG CAG ACC ATG T-3'), was replaced with a hygromycin LacZless-Poly-A-less cassette in reverse orientation under the control of the human ubiquitin promoter, flanked by two loxP sites. When the cassette is removed by Cre excision, a single loxP site flanked by AvrII and XhoI restriction sites that lacks a translational initiation codon. Founder mice were backcrossed into the C57BL/6J background for 10 generations to obtain congenic mice. To remove the hygromycin cassette, heterozygous *Egfl7* males mice were bred to CAG-Cre transgenic females (in a C57BL/6J congenic background, MSKCC Transgenic Core), a strain that retains Cre recombinase activity in mature oocytes, irrespective of *Cre* transgene transmission (Sakai and Miyazaki, 1997). Mice that were identified by genomic PCR as positive for removal of the hygromycin cassette and negative for *Cre* were used.

Initial analyses of mice with the targeted allele were performed using *Egfl7*$^{+/-}$ intercrosses, including genotyping of embryos and pups to examine viability, crown to rump length analyses, and histological examination of placentas. To exclude maternal contribution of a wild-type maternal *Egfl7* allele to the placenta of *Egfl7*$^{-/-}$ conceptuses, we performed all subsequent studies using *Egfl7*$^{-/-}$ intercrosses.

Placentas and embryos were dissected, imaged on Zeiss Discovery.V20 stereoscope, and weighed after removal of excess fluid. Crown-to-rump lengths were measured using ImageJ software (NIH). n=18-28 embryos from at least 3 litters each were used for quantification at each time point (E9.5, E12.5, and E18.5) from *Egfl7*$^{+/-}$ intercrosses, C57BL/6J intercrosses, and *Egfl7*$^{-/-}$ intercrosses. "Pre-placental tissues" = chorion, ectoplacental cone, and decidua. Sex was determined by PCR of genomic DNA for Jarid and SRY using the following primers:

Jarid1d-L: 5' – CTGAAGCTTTTGGCTTTGAG – 3'

Jarid1d-R 5' – CCACTGCCAAATTCTTTGG – 3'

SRY-L: 5' – GAGAGCATGGAGGGCCATG – 3'

SRY-R: 5' – GAGTACAGGTGTGCAGC – 3'

Sequencing

Genomic DNA was amplified using a forward primer complementary to a sequence 384 bp upstream of the 13 bp deletion site with flanking loxP sequence and buffer sequence, and a reverse primer 42 bp downstream of this sequence.
Egfl7 Large Amplicon FWD: 5' – CACAGCATTCCTTTTCCGACA – 3'
Egfl7 Large Amplicon REV: 5' – ATGCTCAGTAGTACCATCTGCTG – 3'

Purified amplified DNA samples were sequenced by the Cornell University Biotechnology Resource Center using Applied Biosystems Automated 3730xl DNA Analyzers. The following sequencing primer was used to confirm the 13bp deletion site and excision of the hygromycin cassette:
Egfl7 Sequencing FWD: 5' – GCCTTTGAATGCTATCCCTGG – 3'

Immunohistochemistry

Placentas were isolated, fixed in 4% paraformaldehyde, and embedded in an OCT:30% sucrose mixture in PBS (2:1). Cryosections were permeabilized in 0.5% Triton-X/0.1% Saponin/PBS (TSP) and blocked with 1% donkey serum in 0.1% TSP/PBS (PBS–TSP). Primary antibodies (CD31, BD Biosciences, 553370, 5 µg ml^{-1}; CYTOKERATIN (DAKO Z0622, 12 µg ml^{-1}; ERG, Abcam, ab110639, 0.17 µg ml^{-1}) were incubated overnight at 4°C in block, followed by incubation with secondary antibodies in block (Alexa488-donkey-α-rat and Cy3-donkey-α-rabbit, Jackson Immunoresearch, 1.5 µg ml^{-1}), and mounted with Prolong Gold + DAPI. IgG controls were used for all immunostaining experiments to ensure specificity. IgG controls were used to ensure specificity. Antibodies used were well established in the literature. Images were acquired using an Axioplan 2 imaging microscope.

For GCM1 immunohistochemistry, sections were stained as above with the following modifications. Primary antibody (GCM1, SantaCruz N-16, 2 µg ml^{-1}), secondary antibody (Alkaline-phosphatase conjugated-α-goat, Jackson Immunoresearch, 0.3 µg ml^{-1}). After washing with TSP, chromogenic detection was performed by NBT-BCIP (Roche) staining in NTMT (100mM NaCl, 100mM Tris-HCl pH9.5, 50mM MgCl2, 1% Tween20, 20µM Levamisole, in H_2O). Samples were post-fixed in 4% paraformaldehyde and imaged using a DKC-5000 (Sony) Digital Photo Camera.

For thick sections, placentas were incubated in 5% low melt agarose (Lonza) for 2 hours at 42°C, and embedded in 3.5% low melt agarose through solidification at room temperature.

Blocks were cut on a vibratome at 100 μm thickness. Agarose was removed and sections were processed for darkfield imaging, confocal imaging, and/or immunostaining as described below.

For hematoxylin and eosin staining, placentas were isolated, fixed in 4% paraformaldehyde, dehydrated through a series of alcohols, and embedded in paraffin. Sections were stained with hematoxylin and eosin, and mounted with Permount (Fisher Scientific). Images were acquired using an Axioplan 2 imaging microscope.

Retrospective Immunostaining of Perfused Placentas

Placenta vibratome sections were blocked for 3 hours in 10% donkey serum in TSP, incubated in CD31 primary antibody (1 μg ml^{-1}) in 5% donkey serum in TSP, overnight at 4°C. Sections were then incubated in 488-donkey-α-rat secondary antibody (1.5 μg ml^{-1}), washed in TSP, and mounted in Prolong Gold using slide wells. IgG controls were used to ensure specificity. Images were acquired using an LSM 880 Laser Scanning Confocal Microscope and processed with Zen or Imaris (Bitplane) software.

Real Time RT-PCR

Pre-placental tissues (chorion, ectoplacental cone, and decidua) were dissected from E8.5 C57BL/6J and *Egfl7*$^{-/-}$ conceptuses, and flash frozen in liquid nitrogen. C57BL/6J and *Egfl7*$^{-/-}$ placentas were isolated at E9.5 and E12.5, and flash frozen in liquid nitrogen. RNA was isolated using Trizol (Invitrogen) and reverse transcribed using qScript cDNA Synthesis Kit (Quanta Biosciences). Gene expression was measured quantitatively using PerfeCTa SYBR Green SuperMix for iQ (Quanta Biosciences). Specific primer sets are listed in **Table S1**. n=4-8 placentas from at least two litters were used for quantification. Differences among target expression were quantified as fold change using the ΔΔCT method and normalized to ß-actin.

For analysis of miR-126 expression, ten nanograms of E12.5 placenta RNA (n=3 placentas from two different litters for each genotype) was reverse transcribed using TaqMan MicroRNA Reverse Transcription Kit (Life Technologies #4366596) with RT primers specific for miR126-3p (*002228*), miR126-5p (*000451*), and control snoRNA234 *(0001234)*. Real Time PCR was performed using TaqMan Universal PCR Master Mix (Life Technologies #4324018) and TaqMan probes for miR126-3p, miR126-5p, and control snoRNA234.

EdU Labeling

Proliferating cells were labeled using the Click-iT EdU Imaging Kit (Life Technologies, C10339). Female C57BL/6J and *Egfl7*$^{-/-}$ mice were subjected to intraperitoneal injection of EdU at 50 µg per gram of body weight at day-12.5 of gestation. After 45 minutes, mice were euthanized and placentas were isolated and fixed in 4% paraformaldehyde overnight. Tissue was cryopreserved, embedded in a 2:1 OCT:30% sucrose mixture, and sectioned for further processing. Sections were permeabilized and EdU detection was carried out according to the manufacturer's protocol. Antibody staining was then performed as described above. Blinded quantification was performed. Approximately every 10th section was used for quantification of labeling, for a total of five sections per placenta (n=3 placentas from two litters per genotype), and analyzed using ImageJ, Metamorph (Molecular Devices) and Prism (GraphPad) software.

Establishing Placental and Embryonic Endothelial Cell Cultures

Placental and embryonic ECs were isolated and activated as previously described (Kobayashi et al., 2010, Poulos et al., 2015), from timed pregnancies of C57BL/6J control and *Egfl7*$^{-/-}$ matings at E10.5. Placentas and embryos were isolated and digested with Collagenase/Dispase (Roche). Placental cell suspensions were lineage depleted (Miltenyi Biotec). ECs were immunopurified using CD31-captured magnetic beads (Life Technologies). Cultures were transduced with a myristoylated-Akt1 expressing lentivirus (Kobayashi et al., 2010), expanded and cultured on fibronectin- (Sigma-Aldrich) coated plates in EC complete culture media (50:50 DMEM:F12, 20%FBS, 1% Pen/Strep/Fungizone, 1% Non-essential amino acids, 0.02M HEPES, 0.02 kU ml^{-1} Heparin, 0.05 mg ml^{-1} EC Growth Supplement). Activation of primary ECs by myr-Akt functions through the recruitment of mTOR and its stimulation of angiogenic growth factors and cytokines. Akt-activated cells from different embryonic and adult vascular beds can be expanded and grown as long-term cultures without additional growth factors or serum, and they retain angiogenic activity but do not senesce (Kobayashi et al., 2010; Poulos et al., 2015). Purity was assessed by immunostaining.

Immunostaining of isolated cell cultures

C57BL/6J and *Egfl7*$^{-/-}$ placental endothelial cells were seeded on coverslips and fixed in 4% paraformaldehyde for 30 min when they reached 90% confluence. Cells were blocked in 5% donkey serum in PBS-TSP for 20 min at room temperature.

Primary antibodies (CD31, 5µg ml^{-1}; CYTOKERATIN, 12µg ml^{-1}; ERG, Abcam, ab110639, 0.17µg ml^{-1}; Ki67, Abcam, ab16667, 1:200; Cleaved Caspase 3, Cell Signaling, 9661S, 1:400)

were incubated in 1% donkey serum in PBS-TSP for 30min at room temperature, followed by incubation with secondary antibodies in 1% donkey serum in PBS-TSP (Alexa488-donkey-α-rat and Cy3-donkey-α-rabbit, 1.5 μg ml^{-1}) for 30 min. Cells were washed and mounted with Prolong Gold + DAPI. IgG controls were used for all immunostaining experiments to ensure specificity. Images were acquired using an Axioplan 2 imaging microscope. The percentage of cells positive for each marker were quantified using ImageJ, Metamorph, and Prism software. Averages of triplicate coverslips from three independent experiments were quantified.

Scratch Wound Assay

Placental and embryonic endothelial cells were grown to confluency and a pipette tip was used to induce a scratch in the monolayer. Debris was removed by washing cells with culture medium. Cells were imaged at 0 hr, 4 hr and 24 hr to observe placental endothelial cell migration and wound closure. The percentage of wound closure was calculated by manual tracing the area of the wound using ImageJ software. Six scratches per genotype from three independent experiments were used for quantification. Cells were fixed in 4% paraformaldehyde at 24 hr and immunostained for Ki67 as above for quantification of proliferation in context of the scratch wound assay. Six scratches per genotype from two independent experiments were used for quantification.

Sprouting Assay

A fibrin gel bead assay was performed to measure endothelial sprouting as previously described (Nakatsu and Hughes, 2008, Tattersall et al., 2016). C57BL/6J and *Egfl7*$^{-/-}$ placental endothelial cells were incubated with Cytodex-3 beads (Sigma) in EC complete culture media at a ratio of 400:1 with gentle agitation for 4 hrs. The beads were plated overnight in EC complete culture media to allow loose endothelial cells to attach to the plate. Beads were removed from the plate, washed, and resuspended in 3 mg ml^{-1} fibrinogen (Sigma) in PBS and 0.15 TI U ml^{-1} Aprotinin (Sigma). Thrombin was added at 0.625 U ml^{-1}, 0.5ml beads-fibrinogen solution was added per well of 24-well plate, and allowed to polymerize for 25 minutes. EC complete culture media was added, and cultures were analyzed at 48 hr and 96 hr for sprout formation. Sprout length and number were quantified (n=11-25 beads from two independent experiments) using ImageJ software.

Proliferation Assay

C57BL/6J and *Egfl7*$^{-/-}$ placental and embryonic endothelial cells were seeded at 7x10^4 cells per well in a 12-well plate. Cells were trypsinized 2 and 4 days after plating, and counted using a hemocytometer. Averages of triplicate counts from three independent experiments were quantified.

Cord formation assay

Placental ECs (10^4 per well) were seeded on 200 µl Matrigel (BD Bioscience), and cultured for 4 hours in 24-well plates. The degree of cord formation and branching interval at 2 hr and 4 hr was analyzed using the Angiogenisis Analyzer for ImageJ (Carpentier et al., 2012). Averages of triplicate wells (n=5 fields per well) from three independent experiments were quantified for each genotype.

Quantitative Analysis of Placental Tissues

Fetal blood space area was quantified on 9 images from CD31 plus CYTOKERATIN immunostained cryosections of the fetal labyrinth zone of placentas (n=3) from at least two litters of C57BL/6J and *Egfl7*$^{-/-}$ mice. Fetal blood space was identified by CD31-positive staining surrounding DAPI-positive nucleated erythrocytes and traced manually using ImageJ software by two blinded, independent researchers. The percentage of fetal blood space of the total area analyzed was quantified.

Morphological quantification of E8.5 and E9.5 tissues was performed on maximum intensity projections of confocal z-stack images and counted or measured/traced manually by two independent blinded researchers using ImageJ software. The percentage of chorion covered by the allantois was analyzed on E8.5 C57BL/6J (n=5) and *Egfl7*$^{-/-}$ (n=4) conceptuses from at least two litters each. The number and length of chorionic invaginations was analyzed on E9.5 placentas (n=3) from at least two litters of C57BL/6J and *Egfl7*$^{-/-}$ mice. Length of each invagination was measured from the base of the CYTOKERATIN-positive chorion to the tip of the CD31-positive invading vessel.